Micro Electro Mechanical Systems Lab
Tanaka Shuji Laboratory

MEMS Research in S. Tanaka Lab, Tohoku University

Shuji Tanaka, Professor, IEEE Fellow
Department of Robotics
Microsystem Integration Center
Tohoku University
mems@tohoku.ac.jp

mems tohoku 検索

Tohoku University in Sendai

Sendai is the largest city in the north east area of Japan, where Tohoku University is located. Sendai and Tokyo are connected by bullet trains in 1.5 hours.

Tohoku University was established as Japan's third national university in 1907. Tohoku University is proud to be ranked among Japan's leading universities.

MEMS Facilities in Aobayama Campus

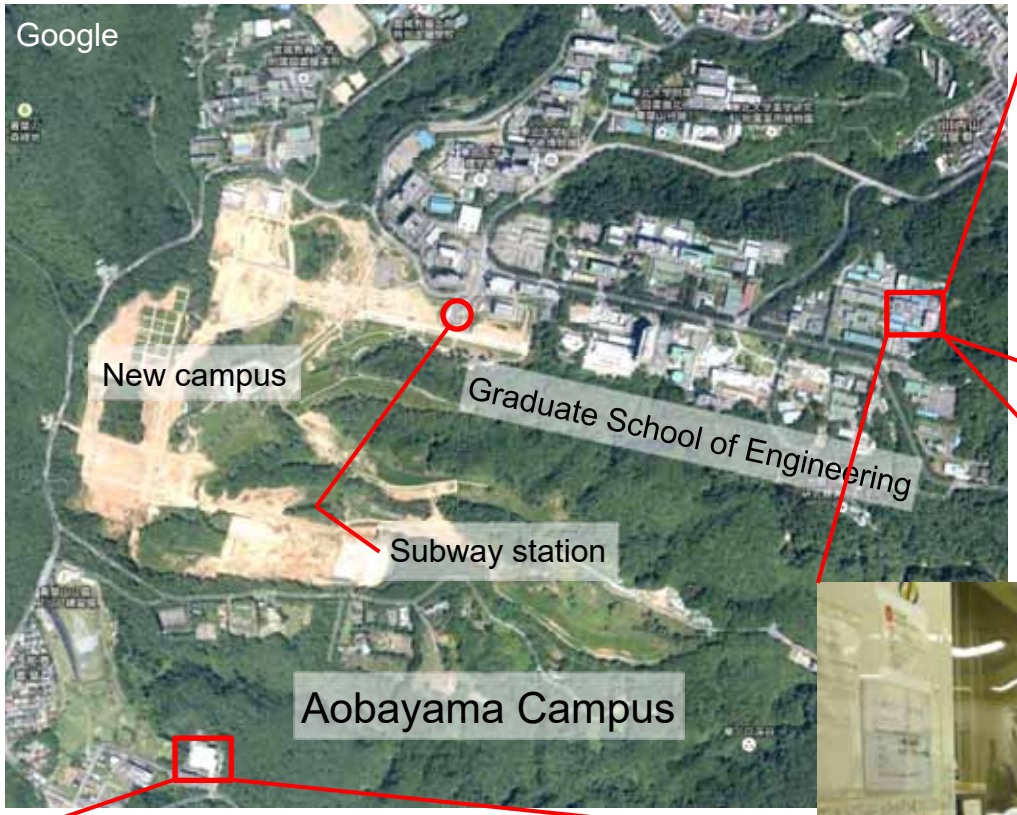

Micro/Nano-Machining Research and Education Center (MNC)

J. Nishizawa Memorial Research Center

S. Tanaka Laboratory Cleanroom

Industry-Relevant R&D System in Tanaka Lab

From basic research to practical development for industrial customers

S. Tanaka Lab's cleanroom

Micro/Nano-Machining Research & Education Center (MNC)

Microsystem Integration Center (μSIC)

Small piece

4 inch wafer

6 inch wafer

Micro Electro Mechanial Systems lab
Tanaka Shuji Laboratory

μSIC
Micro System Integration Center

Areas of strength

Physical sensors, Piezoelectric devices, Acoustic wave devices (SAW and BAW), Wafer-level packaging, MEMS-LSI integration, Hetero-integration etc.

Examples of commercialization

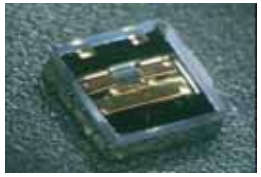

RF-MEMS switch

Vacuum sensor

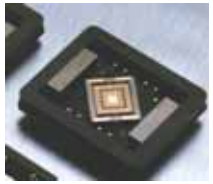

Optical scanner

Ultra-small GT generator

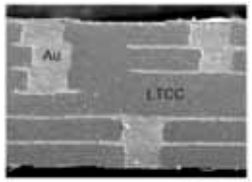

LTCC MEMS packaging

ALD tool

Wafer bonder

S. Tanaka Laboratory

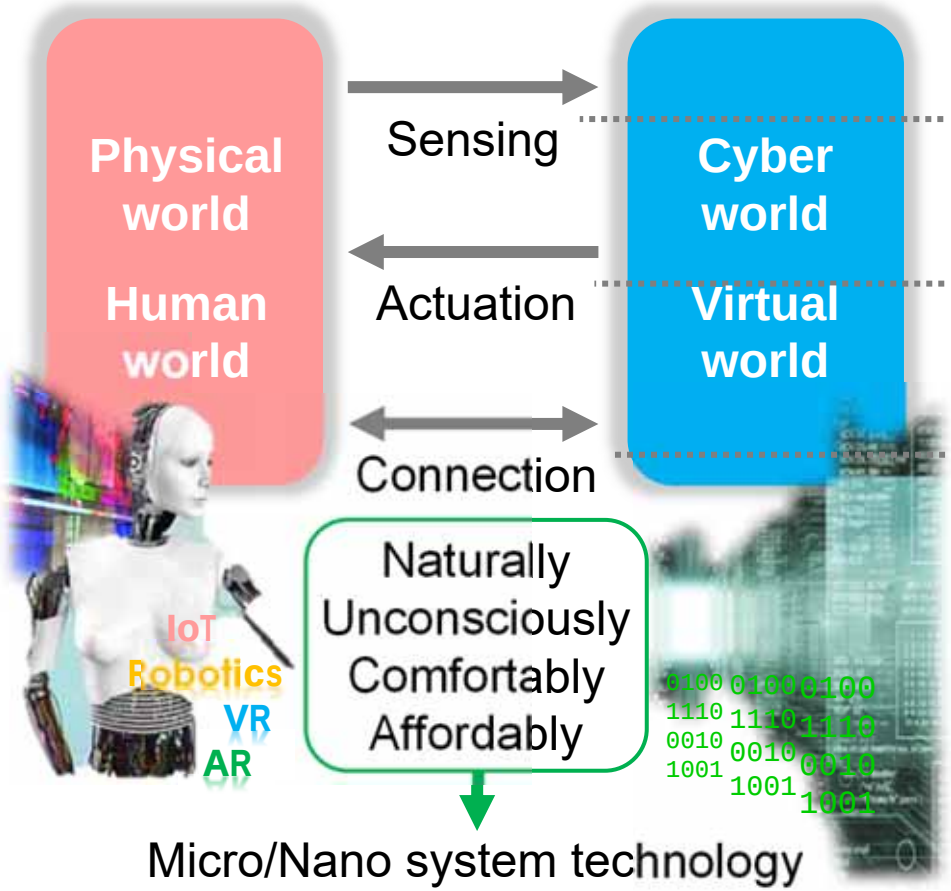

Research topics in 2018-2019

e.g. Tactile sensor, Gyroscope, Ultrasonic sensor, Microphone

e.g. Micromirror, Optical stage, RF MEMS switch

e.g. SAW and BAW filter

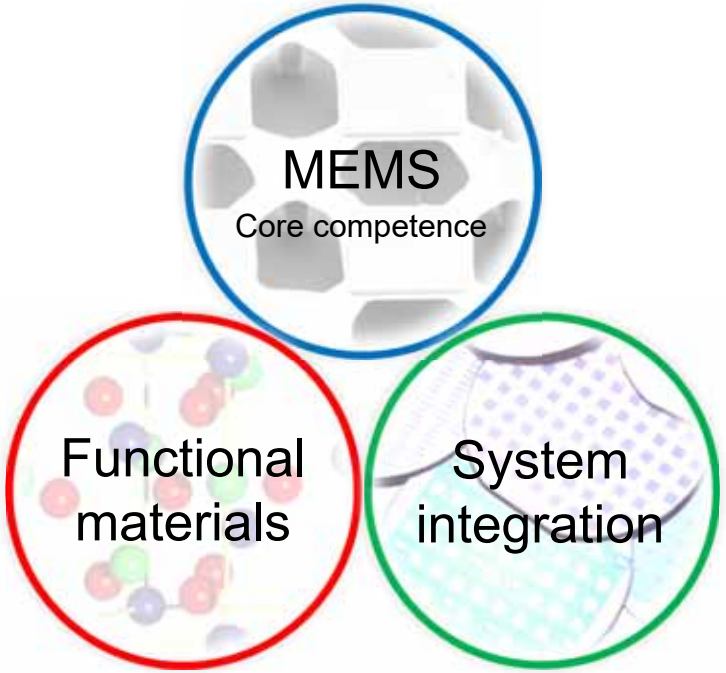

Recent research topics

Gyroscope, Ultrasonic transducer, Tactile sensor, Haptic device, MEMS speaker, Micromirror device, MEMS actuator stage, Acoustic wave device, Piezoelectric thin film, Packaging, ALD etc.

Whole Angle Gyroscope

mems tohoku

検索

Applications Need High Performance Gyro

VR with position tracking
(The VOID)

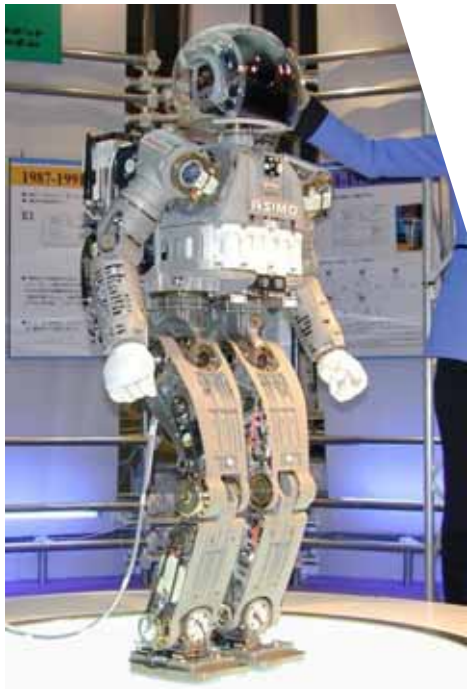

Robot “Asimo”
(Honda Motor)

Autonomous car (Nissan Motor)

Autopilot indoor drone (DARPA)

Performance of Gyroscopes

S. Tanaka, Intl. Conf. "Global/Local Innovations for Next Generation Automobiles" (2015)

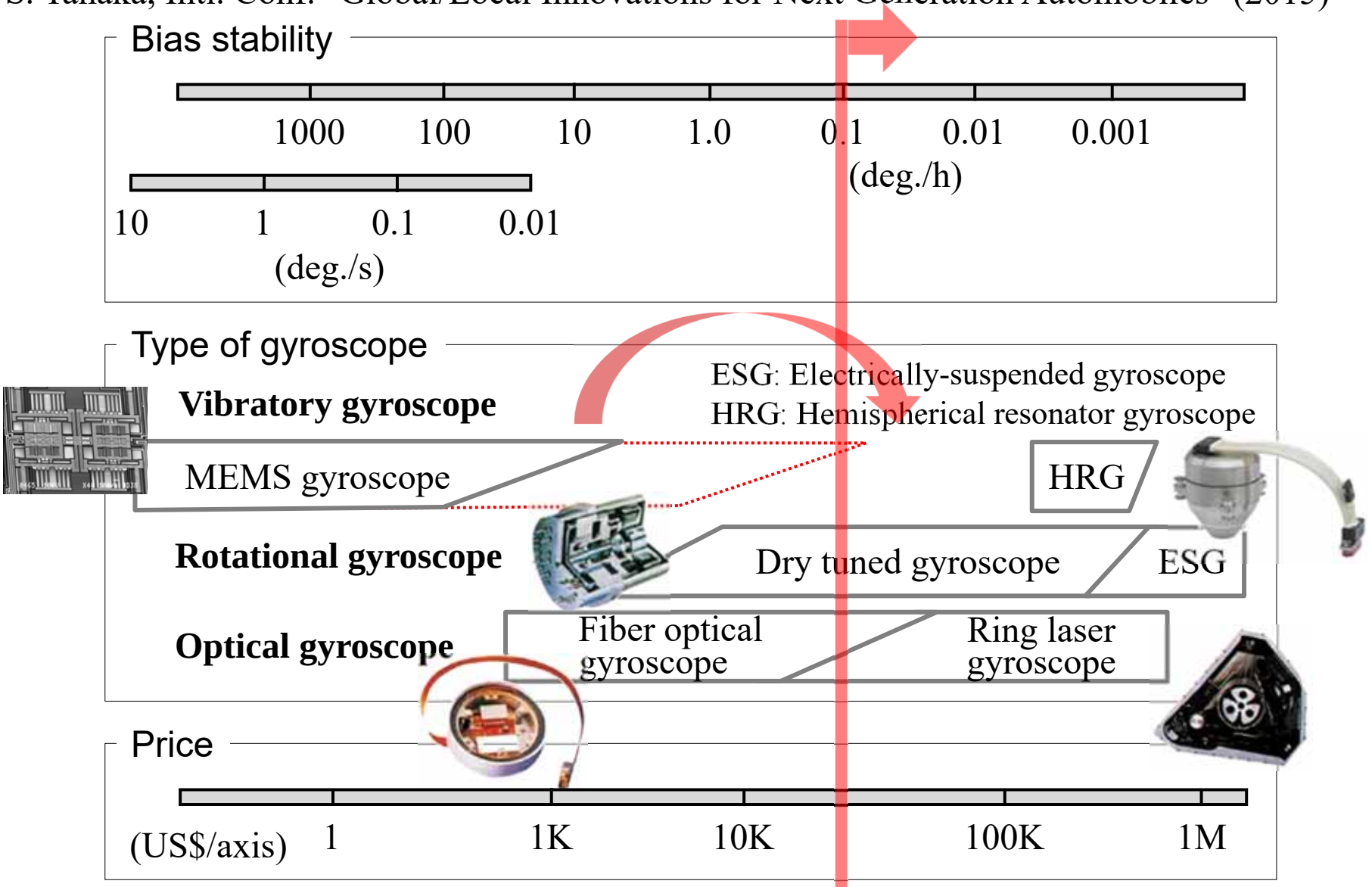

DTG, FOG, RLGの図：多摩川精機　HRGの図：Northrop Grumman

FM / Whole Angle Mode Gyroscope

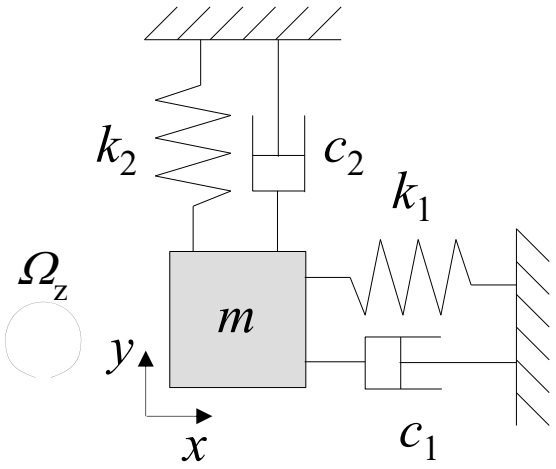

$$\begin{cases} \ddot{x} + \dfrac{c_1}{m}\dot{x} + [\dfrac{k_1}{m} - \Omega_z^2]x = 2\,\Omega_z\dot{y} \\ \ddot{y} + \dfrac{c_2}{m}\dot{y} + [\dfrac{k_2}{m} - \Omega_z^2]y = -\,2\,\Omega_z\dot{x} \end{cases}$$

Coriolis force

$$\lambda^2 = (\omega^2 + \Omega_z^2 + \frac{\Delta\omega}{4}) \pm \sqrt{\Delta\omega^2(\omega^2 + \Omega_z^2) + 4\omega^2\Omega_z^2}$$

Assuming $\Delta\omega = \omega_1 - \omega_2 = 0$ (Mode match)

$\lambda_1 = \omega + \Omega_z \quad \lambda_2 = \omega - \Omega_z$ ⇨ $\lambda_1 - \lambda_2 = 2\Omega_z$

Temperature sensitive

Temperature insensitive

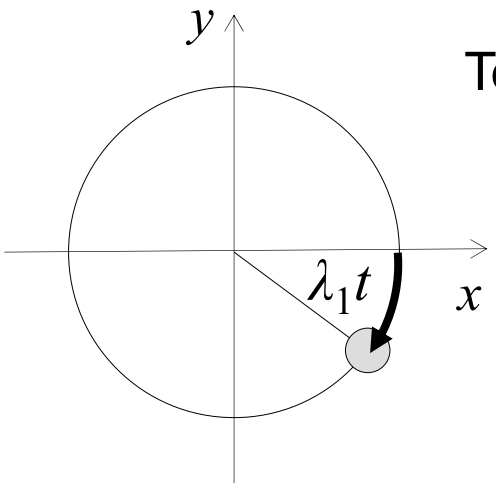

CW mode ($\lambda_1 = \omega + \Omega_z$)

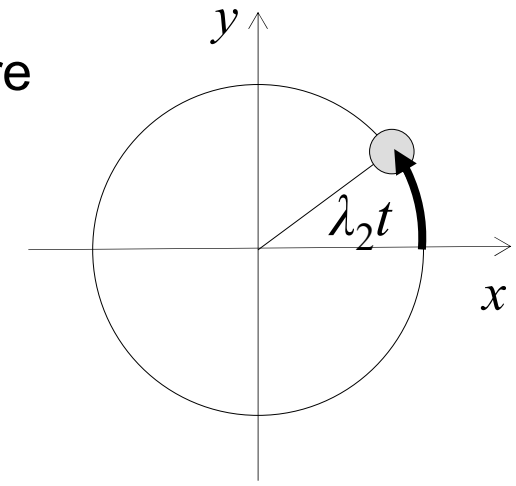

CCW mode ($\lambda_2 = \omega - \Omega_z$)

Whole Angle Mode Type Gyro

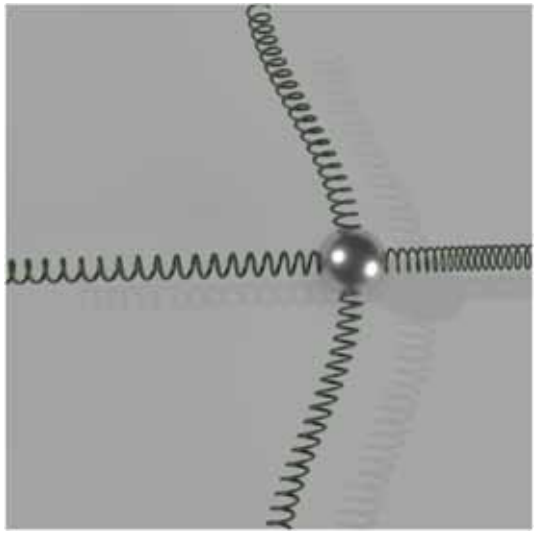

CW mode ($\lambda_1 = \omega + \Omega_z$)

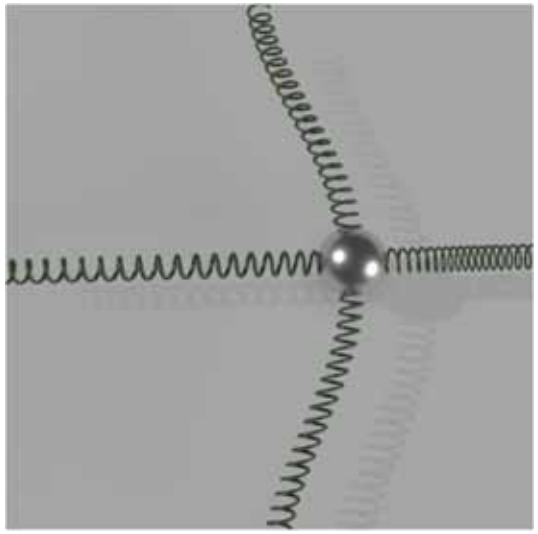

CCW mode ($\lambda_2 = \omega - \Omega_z$)

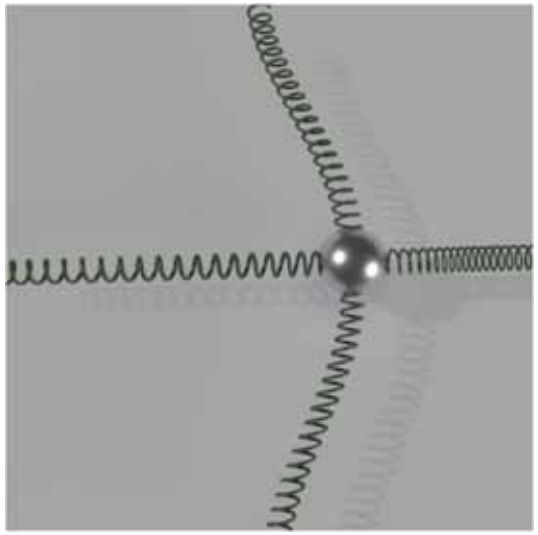

CW + CCW mode ($\Delta\Phi$ = 0°)

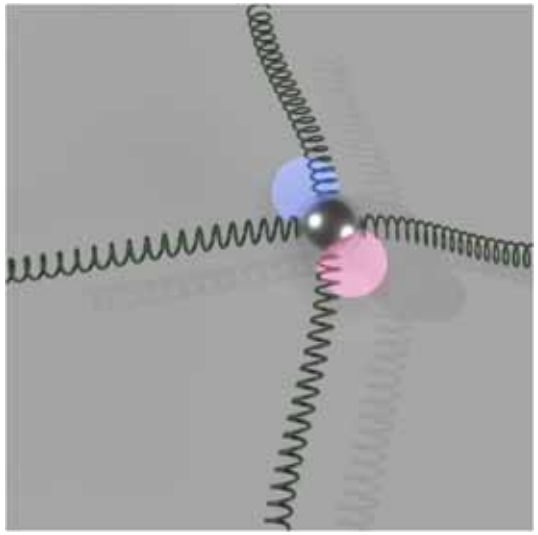

CW + CCW mode ($\Delta\Phi$ = 90°)

Whole Angle Mode Gyroscope

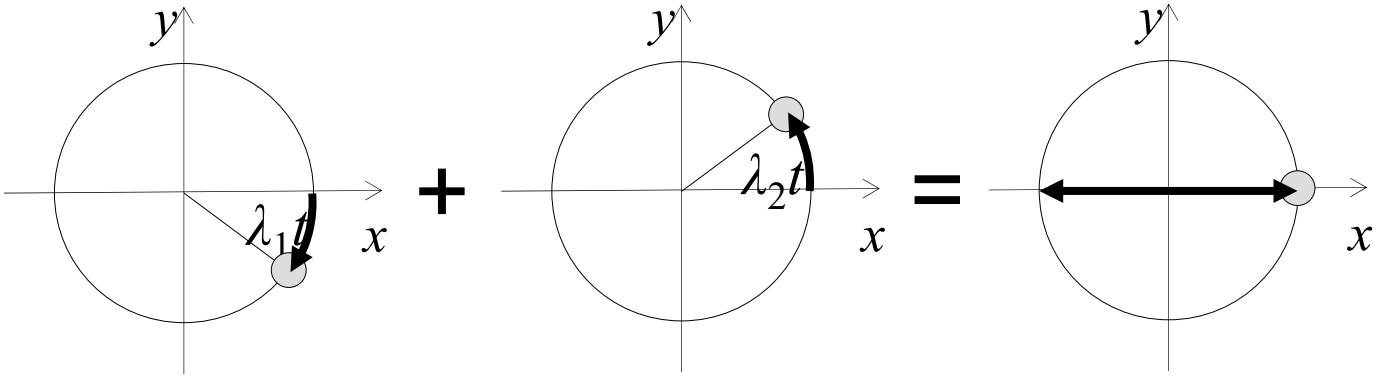

CW mode　　CCW mode　　Liner vibration

Foucault pendulum

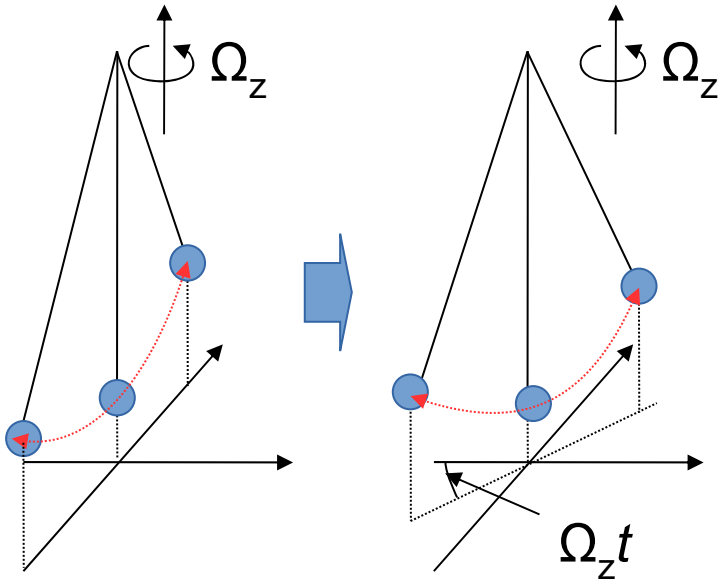

System of Whole Angle Mode Gyroscope

T. Tsukamoto, S. Tanaka, Tohoku University, IEEE MEMS 2017, IEEE Inertial 2017

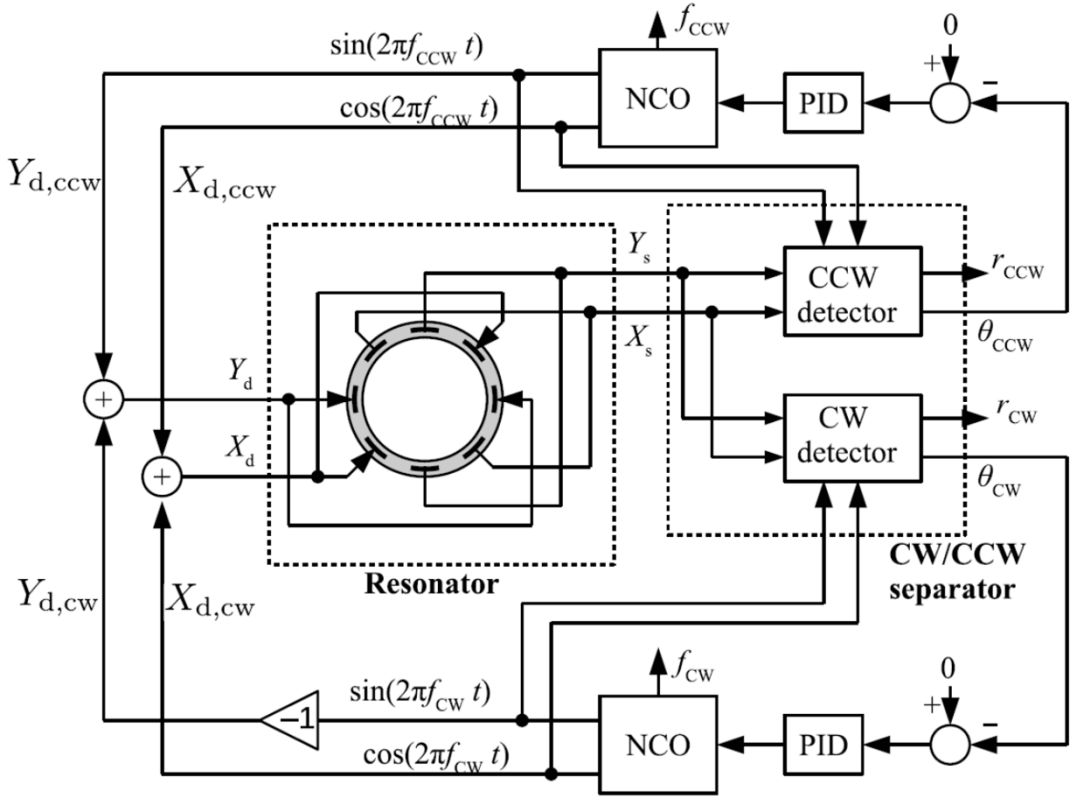

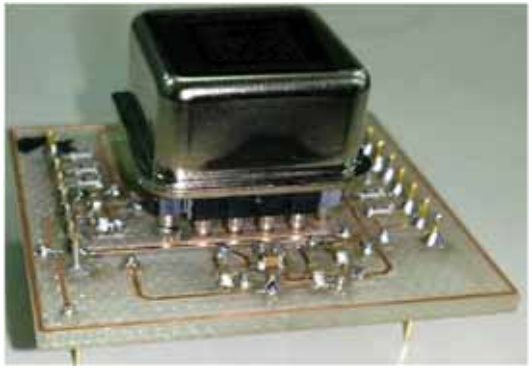

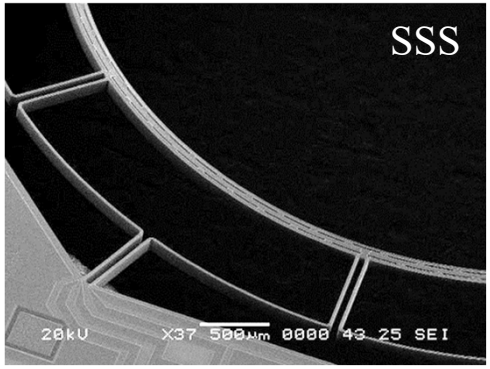

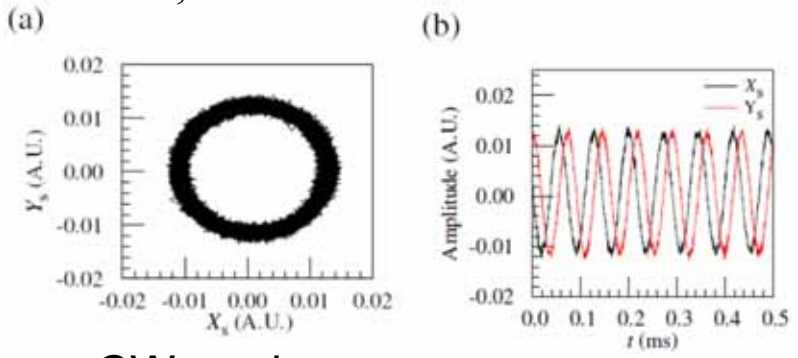

CW mode

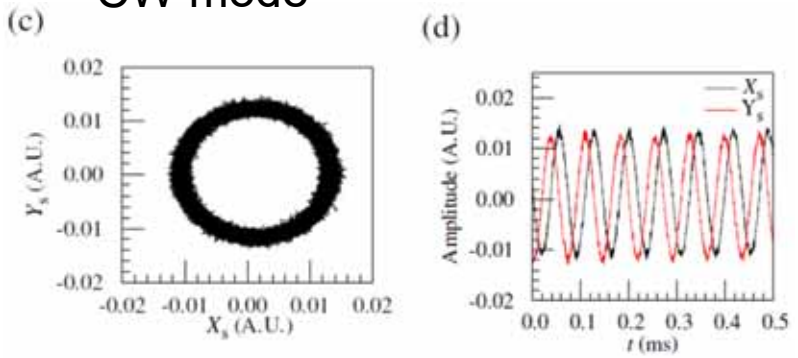

CCW mode

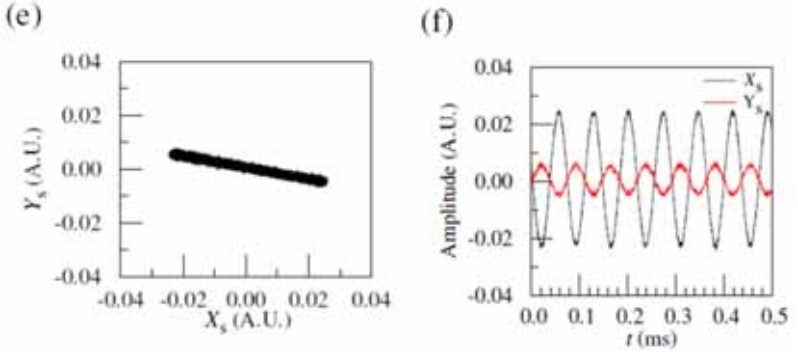

CW + CCW modes

Foucault Pendulum Type Gyroscope

T. Tsukamoto, S. Tanaka, Tohoku University, IEEE MEMS 2017, IEEE Inertial 2017

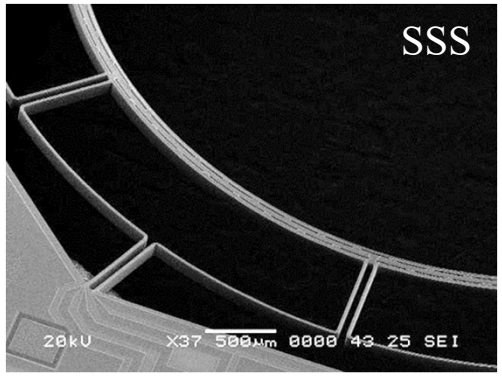

MEMS ring resonator
in the vacuum package

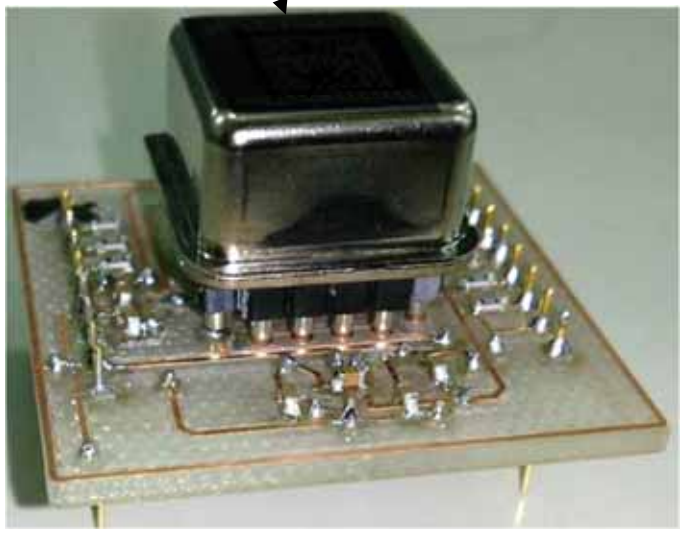

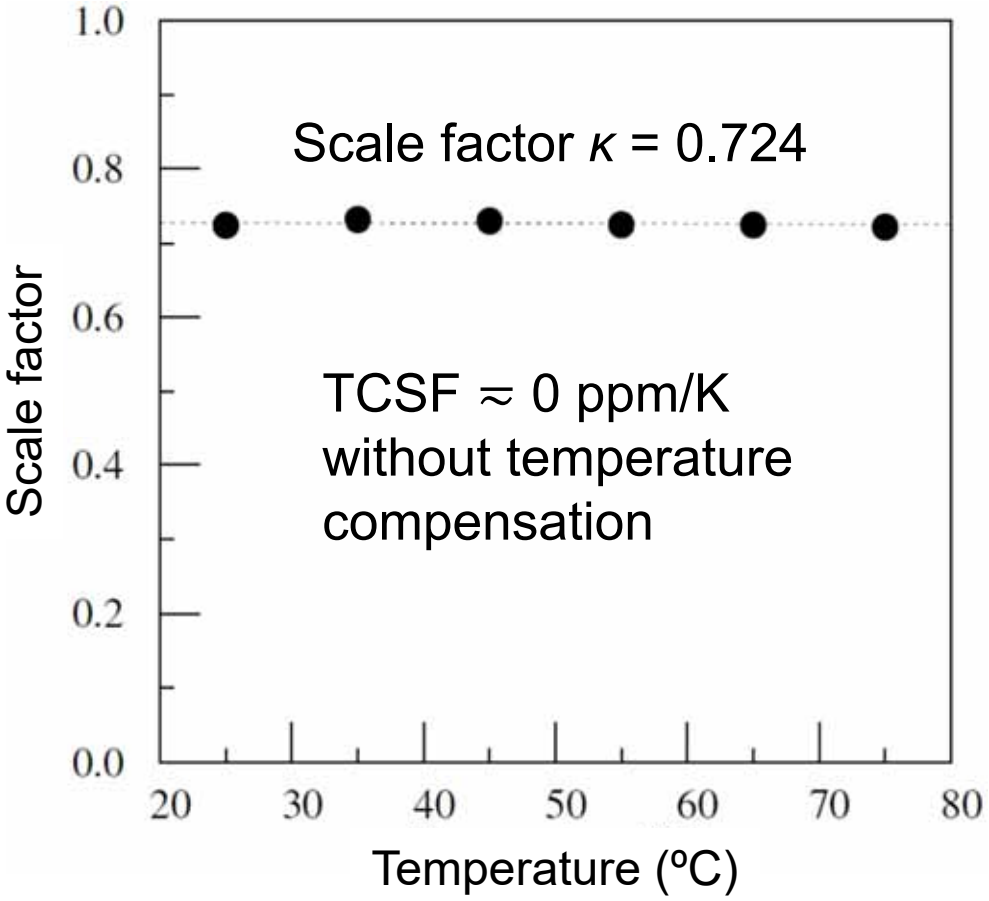

Temperature characteristic of scale factor (TCSF)

Error ±26 ppm

Performance of Whole Angle Mode Gyroscope

T. Tsukamoto, S. Tanaka, Tohoku University, IEEE Inertial 2018

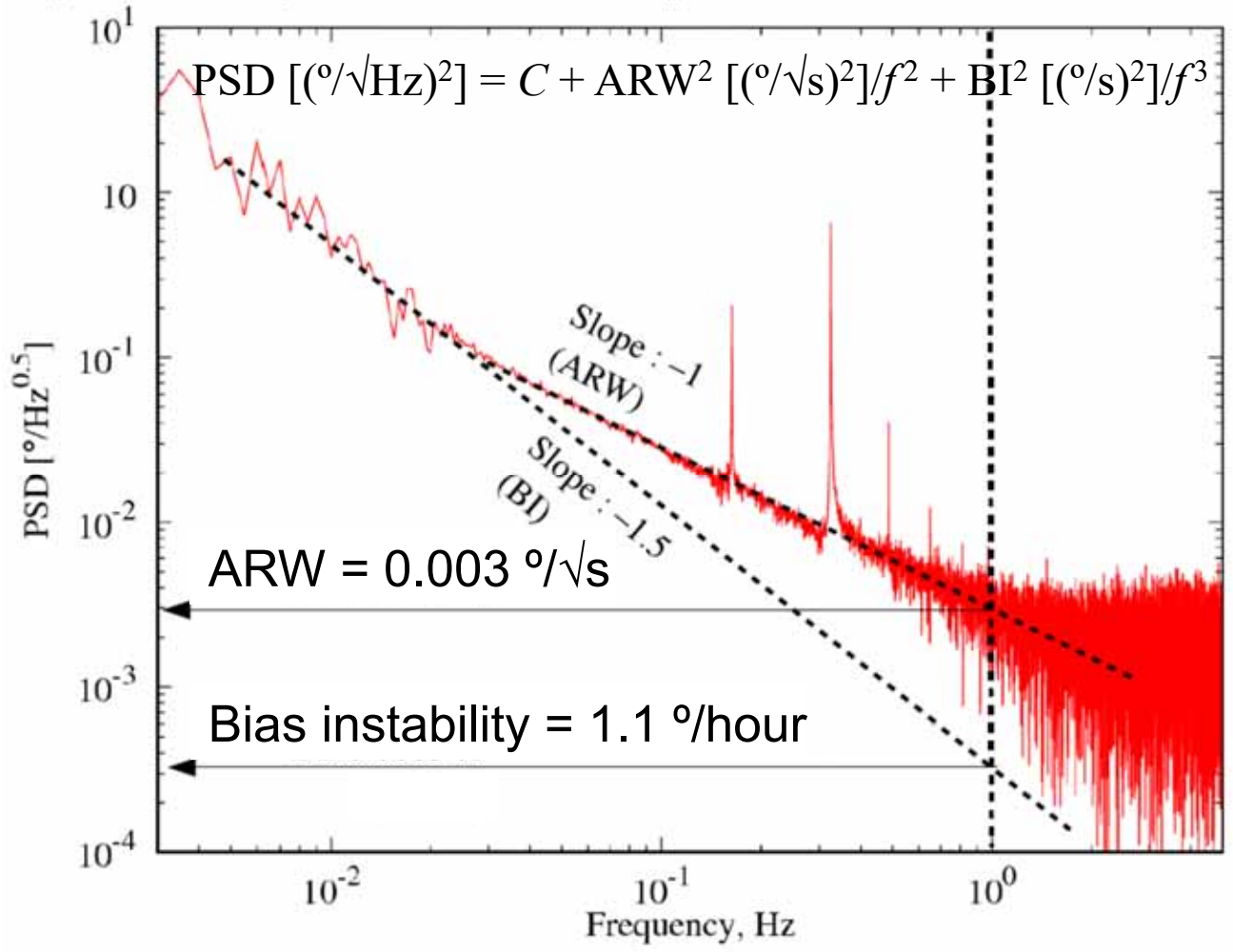

PSD of angle with virtual rotation after the subtraction of virtually rotated angle

Electrical mismatch compensation and virtual rotation are “tricks” not explained in this presentation.

Piezoelectric MEMS

mems tohoku

検索

Micromirror Device (Stanley Electric)

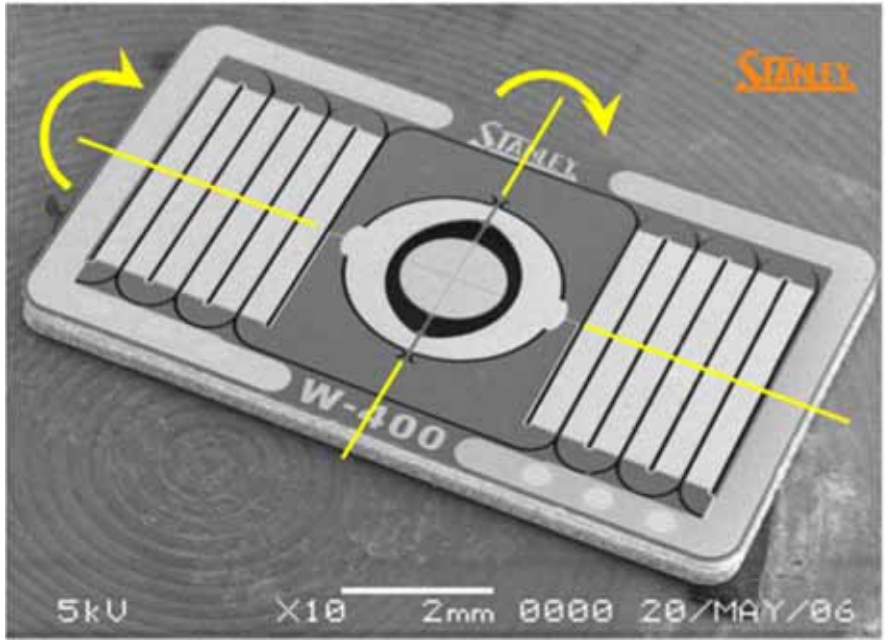

Stanley, 応用物理学会2014春, 17p-E9-7

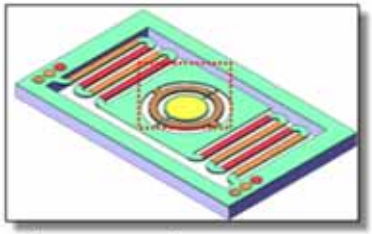

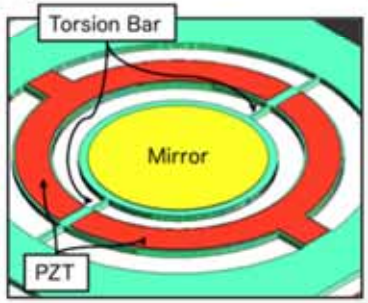

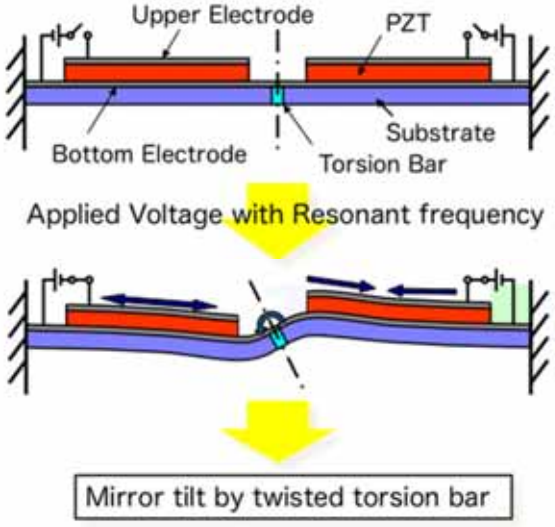

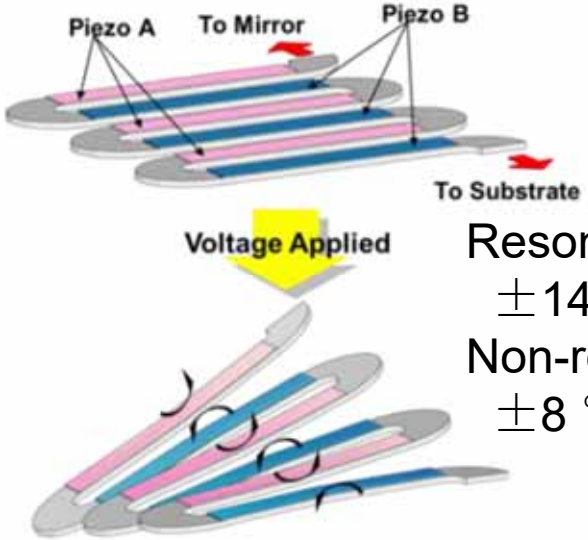

Resonant axis:
±14 °
Non-resonant axis:
±8 ° at 60 V

Epitaxial PZT Film

S. Yoshida *et al.*, IEEE Trans. Ultrason. Ferroelect. Freq. Contr., 61 (2014) 1552-1558
S. Yoshida *et al.*, Sens. Actuators A, 239 (2016) 201-208
P. N. Thao *et al.*, Jpn. J. Appl. Phys., 56 (2017) 127201

PZT (a axis: 0.404 nm, c axis: 0.415 nm)

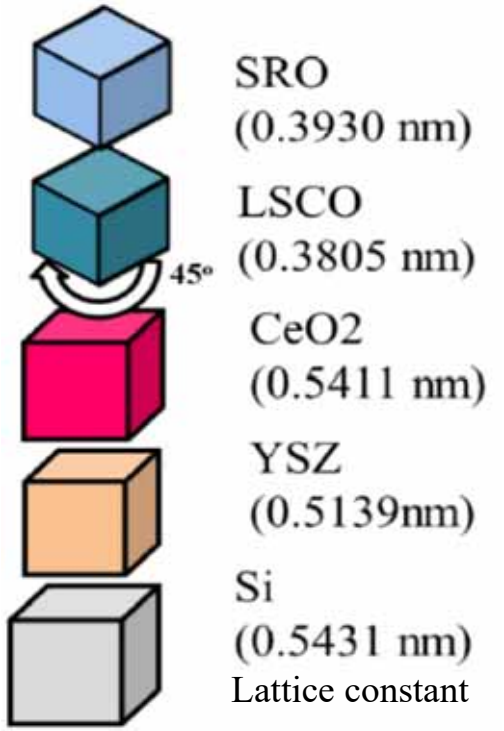

Oxide buffer layer

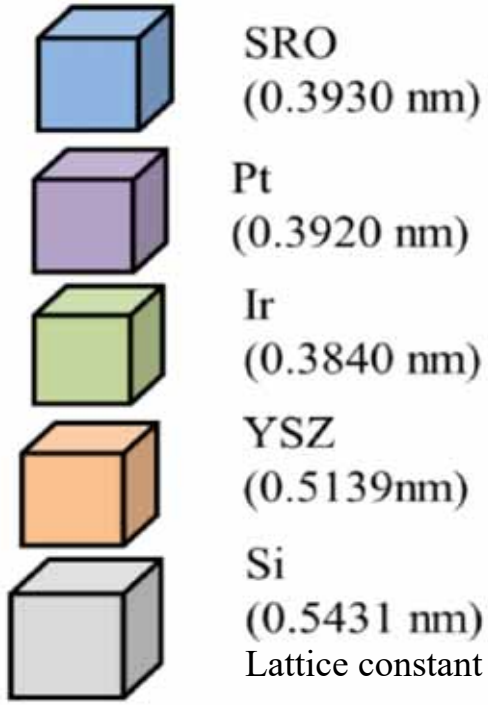

Metal buffer layer

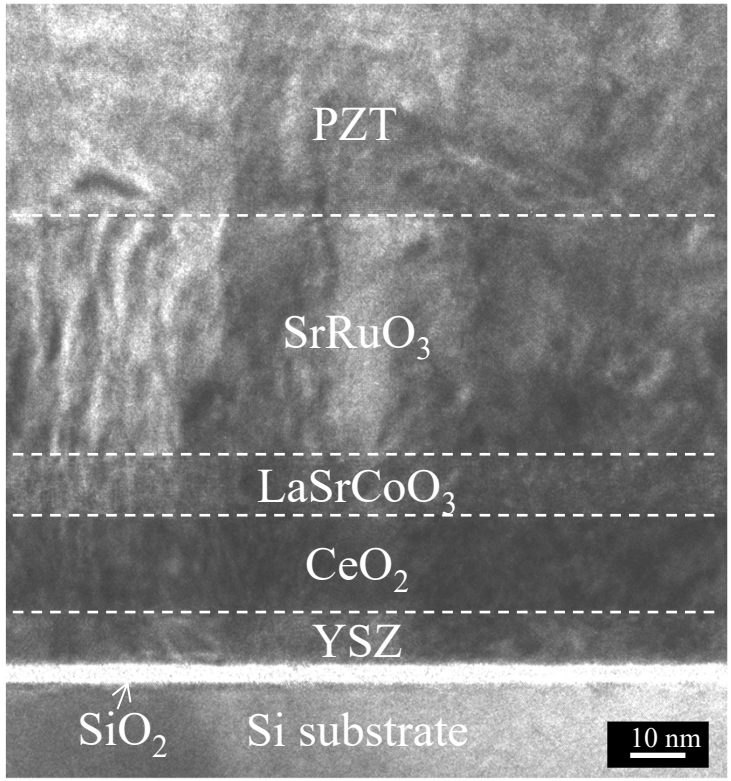

TEM image

$e_{31,f} = -14$ C/m^2, $\varepsilon_{r33} = 200\sim300$, $T_c > 500$ºC

Comparison of Sputtered PZT Thin Films on Si

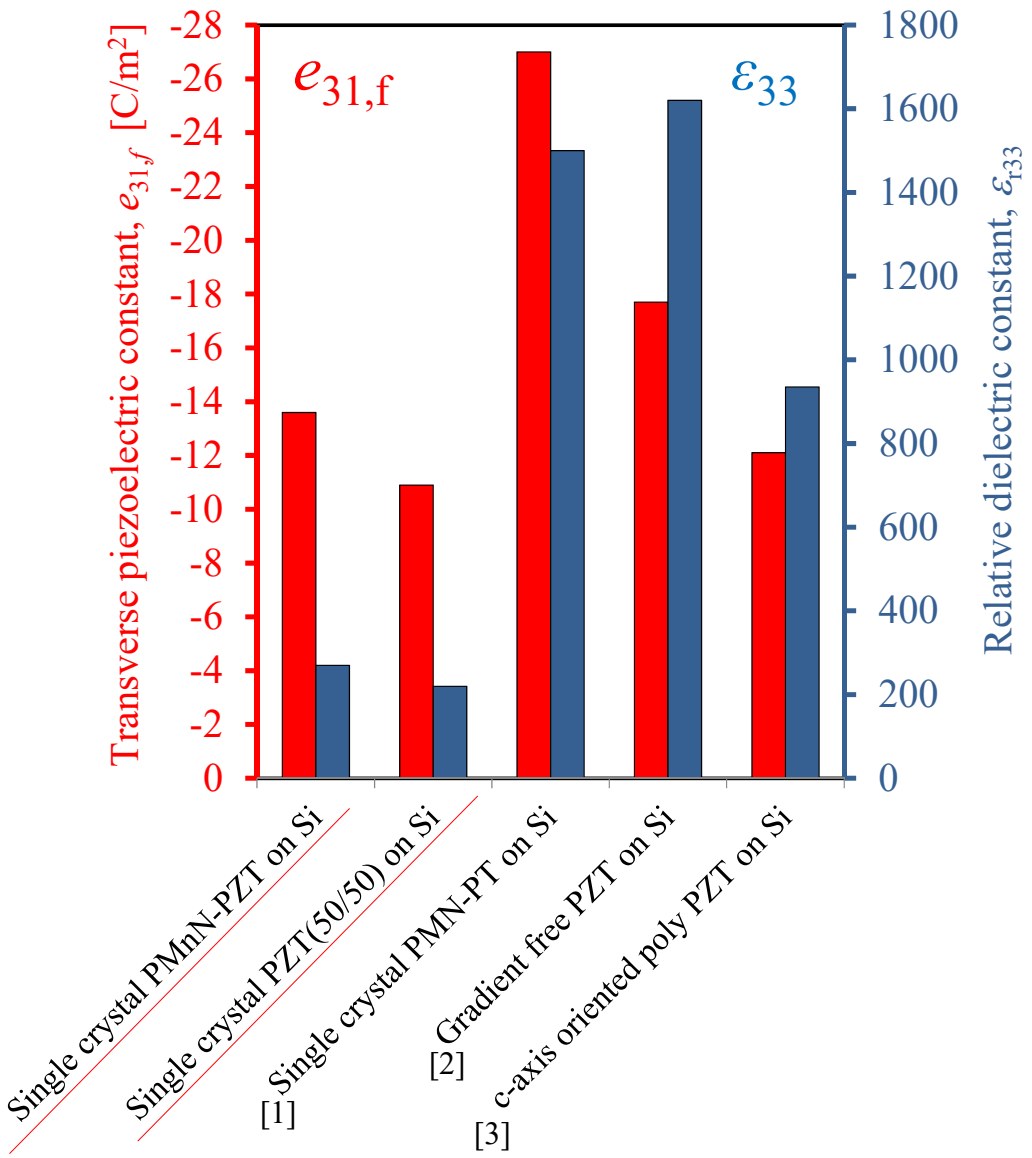

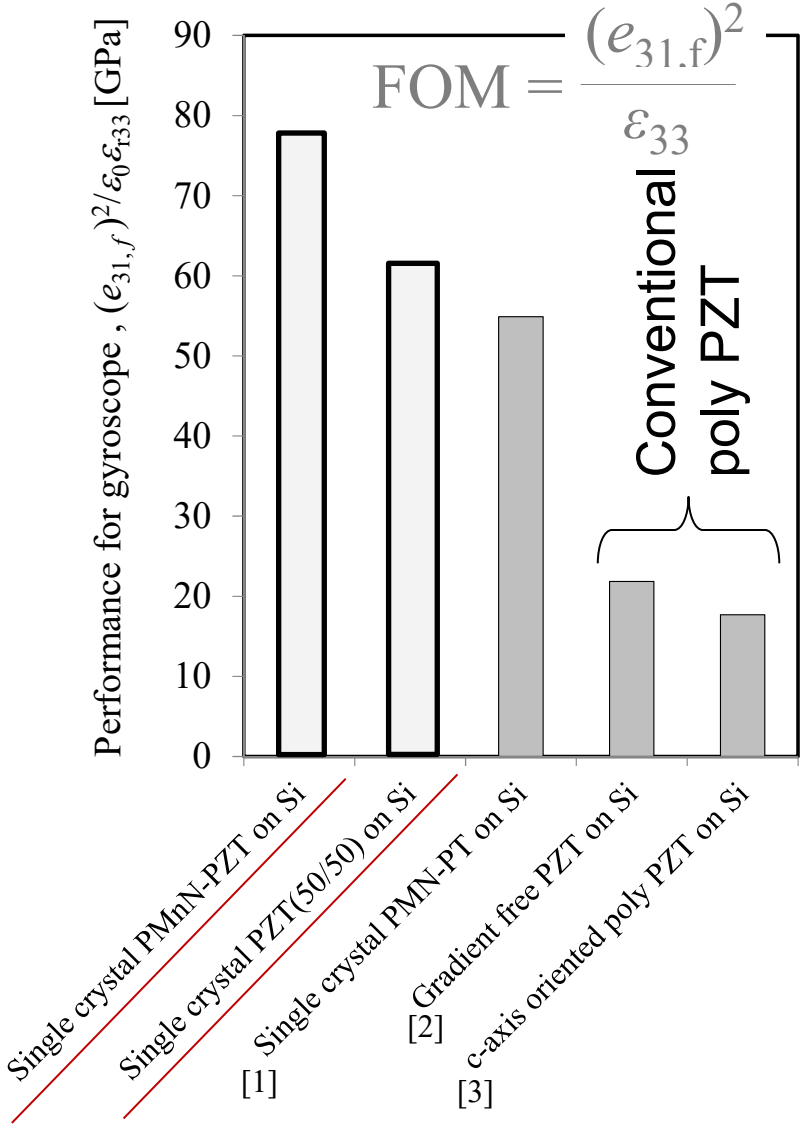

[1] S. H. Baek … B. Eom, Science **334,** 958 (2011) [2] F. Calame, P. Muralt, Appl. Phys. Lett. 90, 062907 (2007)
[3] N. Ledermann et al., Sens. Actuators A, 105, 162 (2003)

pMUT Using Epitaxial PZT

Z. Zhou, S. Yoshida, S. Tanaka, Transducers 2017, Sens. Actuators A, 266 (2017) 352-360

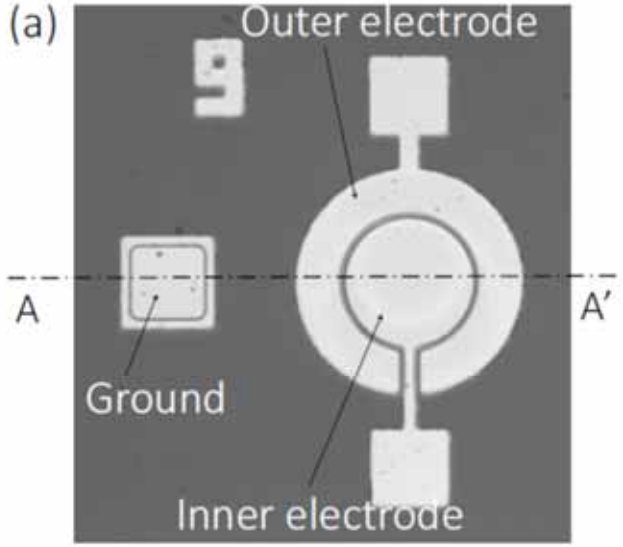

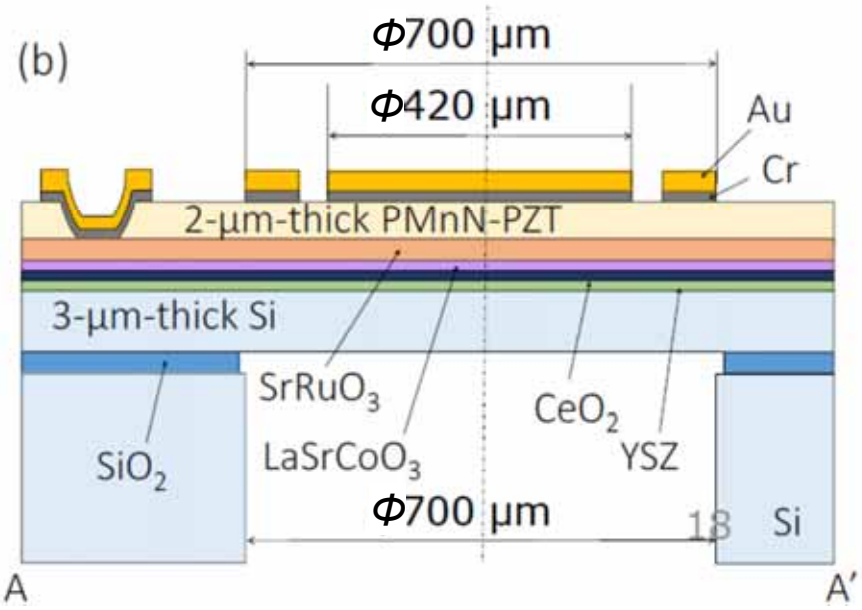

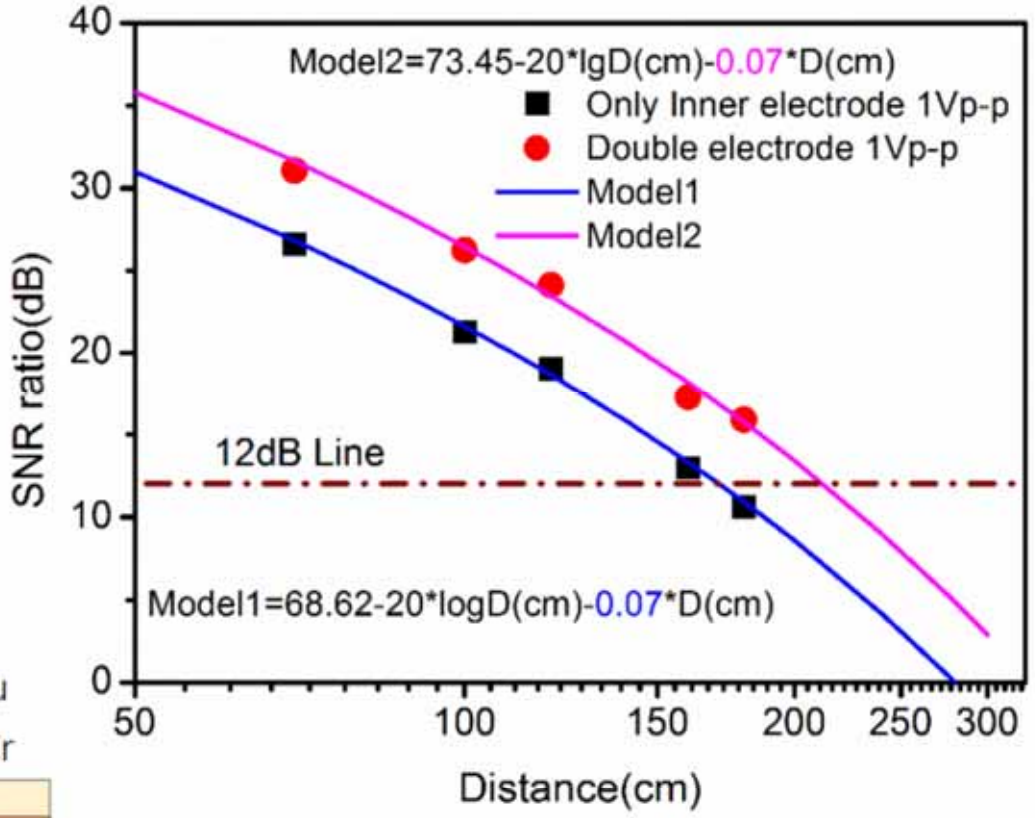

$$SNR \propto \frac{V_{tx}^2 \times e_{31,f(Tx)}^2 \times e_{31,f(Rx)}^2}{\alpha\ \omega_0^2 \varepsilon_{(Rx)}^2 + \beta\ e_{31,f(Rx)}^2}$$

pMUT for Range Finder and Fingerprint Sensor

Z. Liu *et al.*, Transducers 2019, Sensors and Actuators A, 312 (2020) 112145

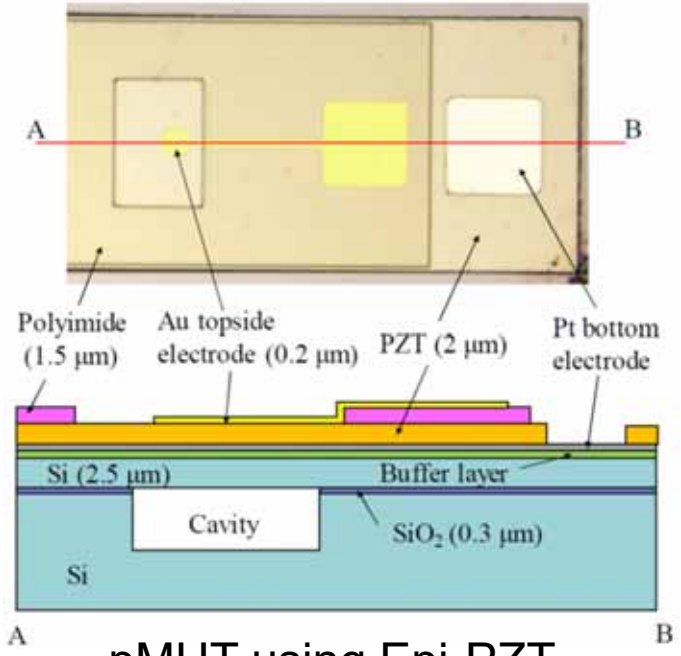

pMUT using Epi-PZT

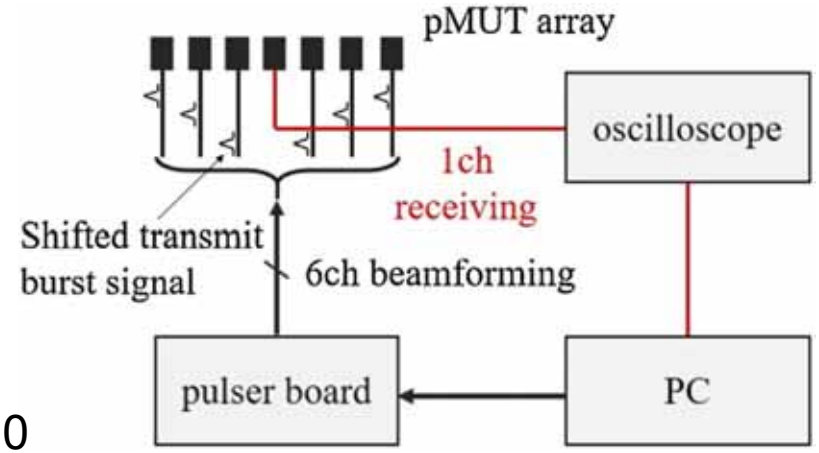

(a)

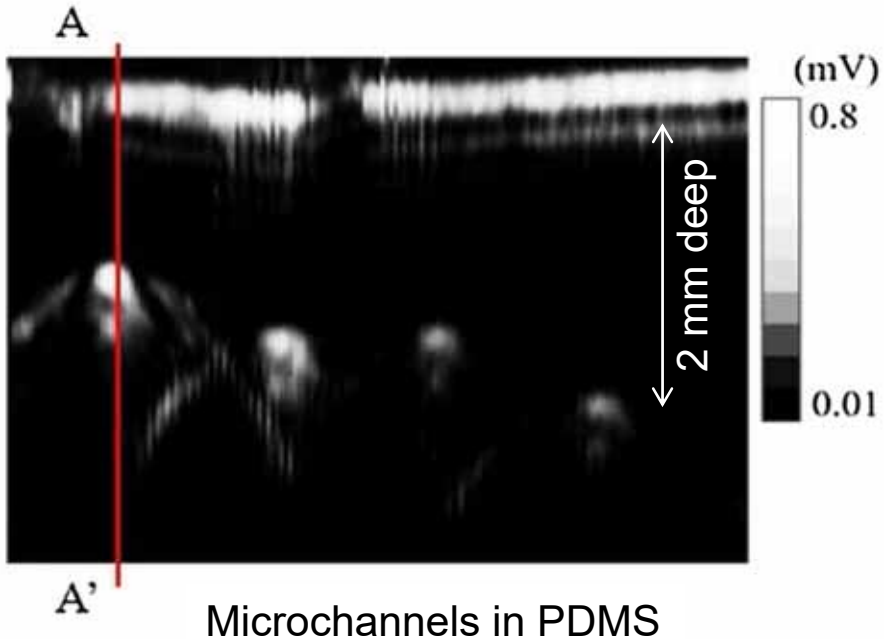

Microchannels in PDMS

(b)

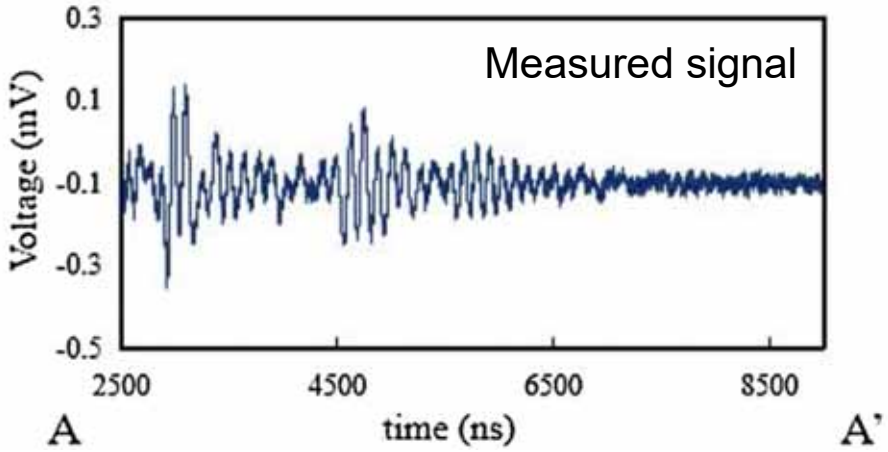

RF Acoustic Wave Devices

TV White Space Cognitive Radio

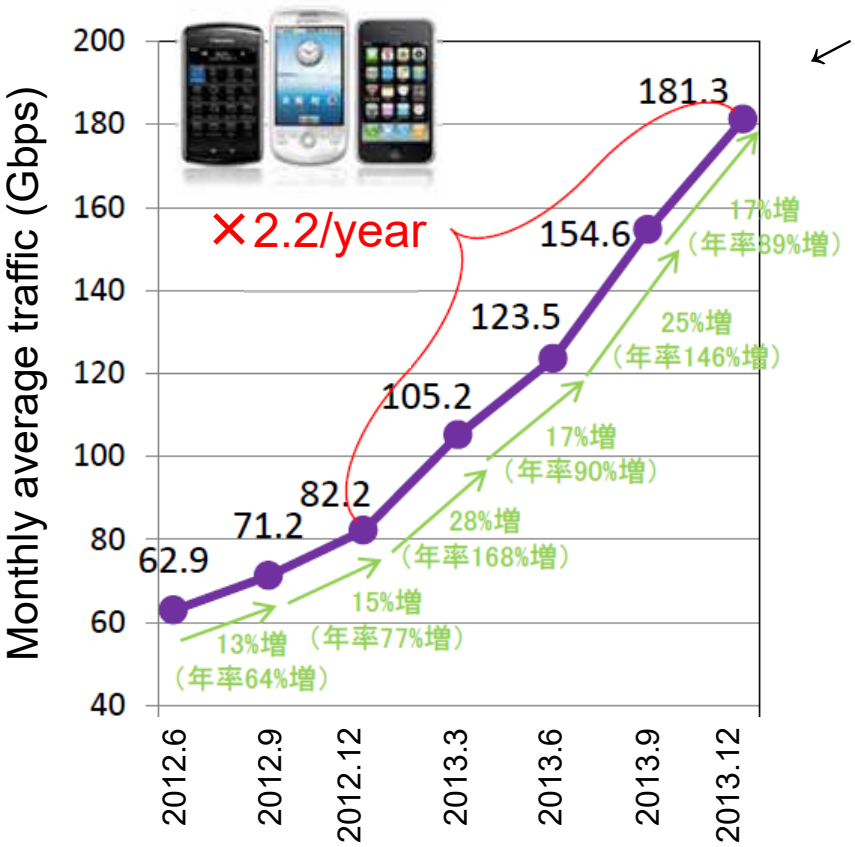

↙ Monthly average traffic of mobile communication in Japan

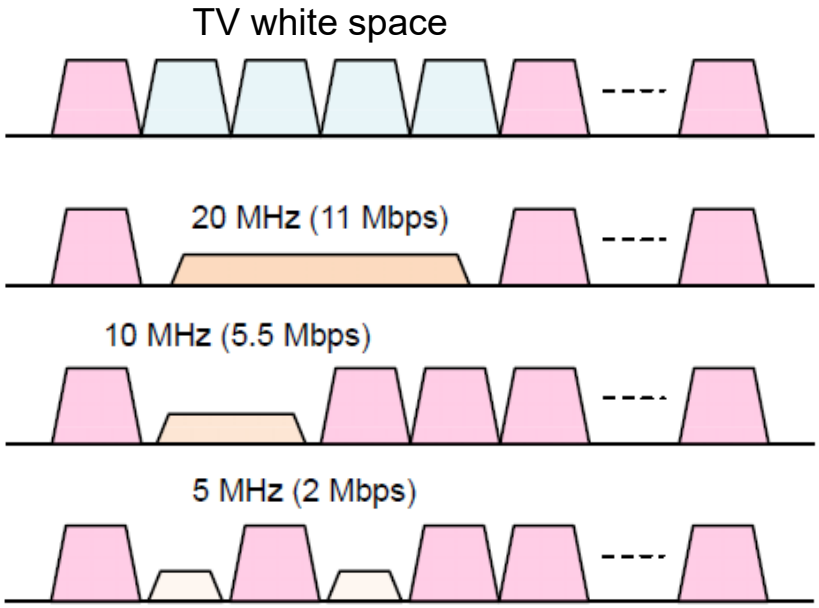

TV white space cognitive radio communication (IEEE 801.11af)

Digital TV band

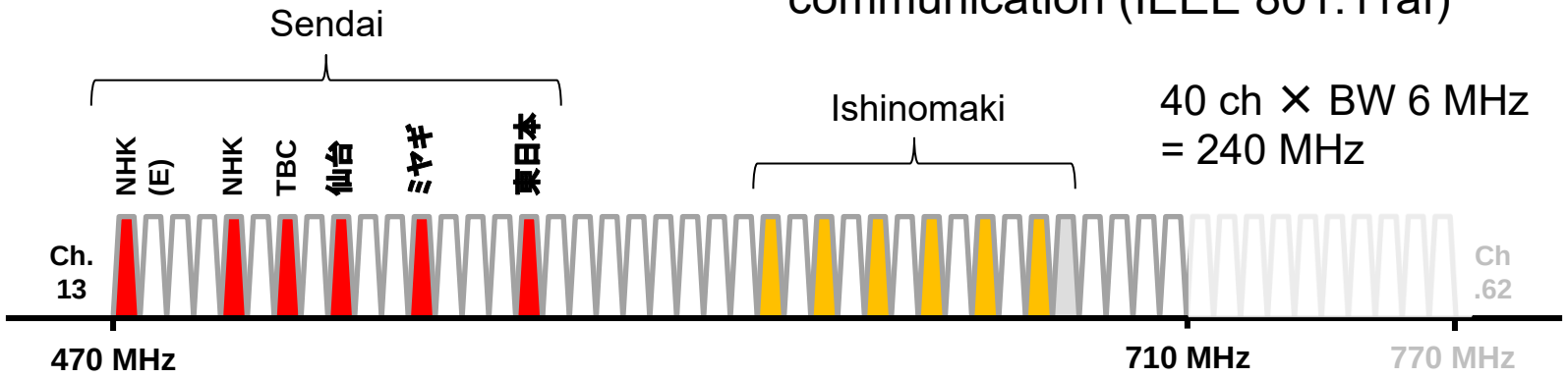

40 ch × BW 6 MHz = 240 MHz

Design of Tunable SAW Filter

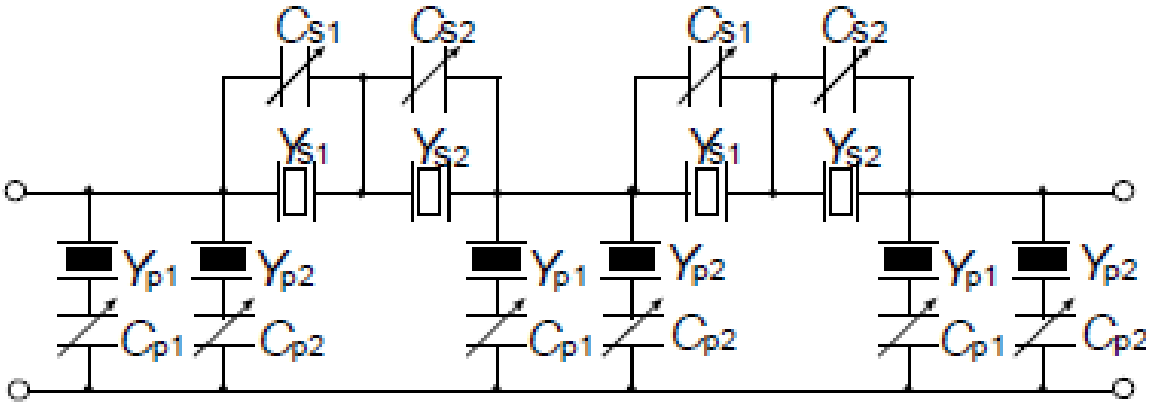

Y: SAW resonator
C: Varactor

10 SAW resonators and
10 varactors integrated
on 42YX $LiTaO_3$

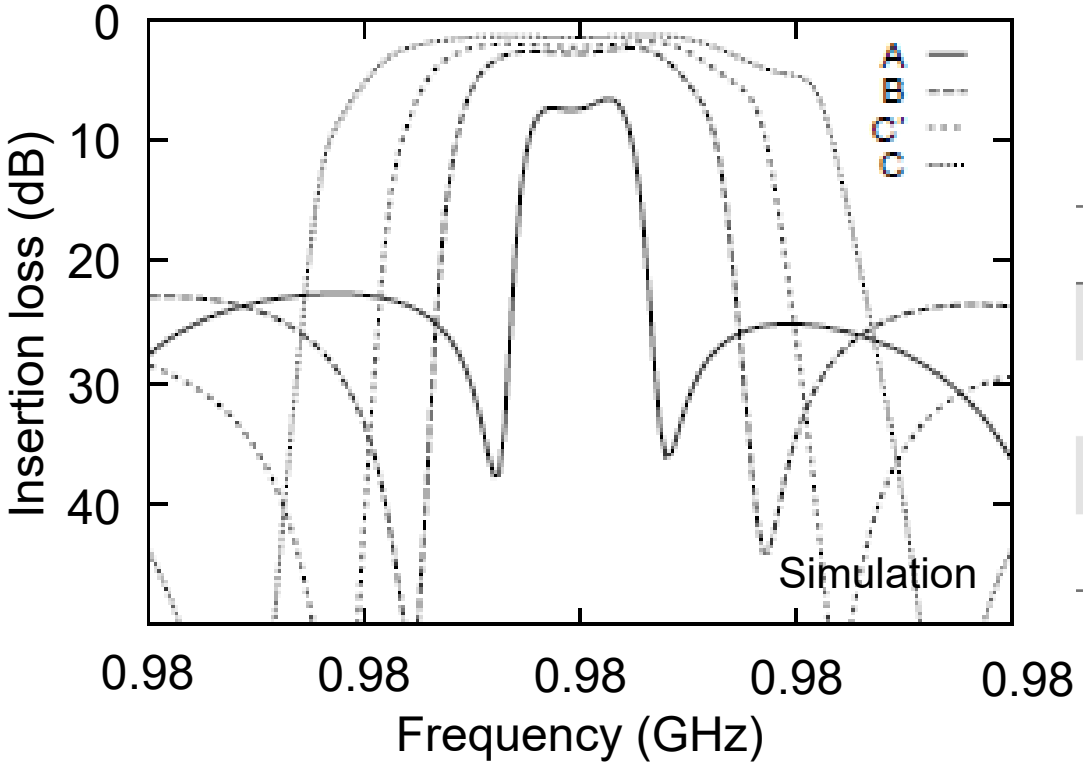

Relationship between capacitance and bandwidth

	A		B		C'	C
C_{p1}	Small	←				Large
C_{p2}	Large	←				Small
C_{s1}	Small	←				Large
C_{s2}	Large	←				Small

M. Inaba, T. Ohmori, K. Hashimoto (Chiba Univ.), Jpn. J. Appl. Phys., 52 (2013) 07HD05

Tunable SAW Filter with Integrated Varactors

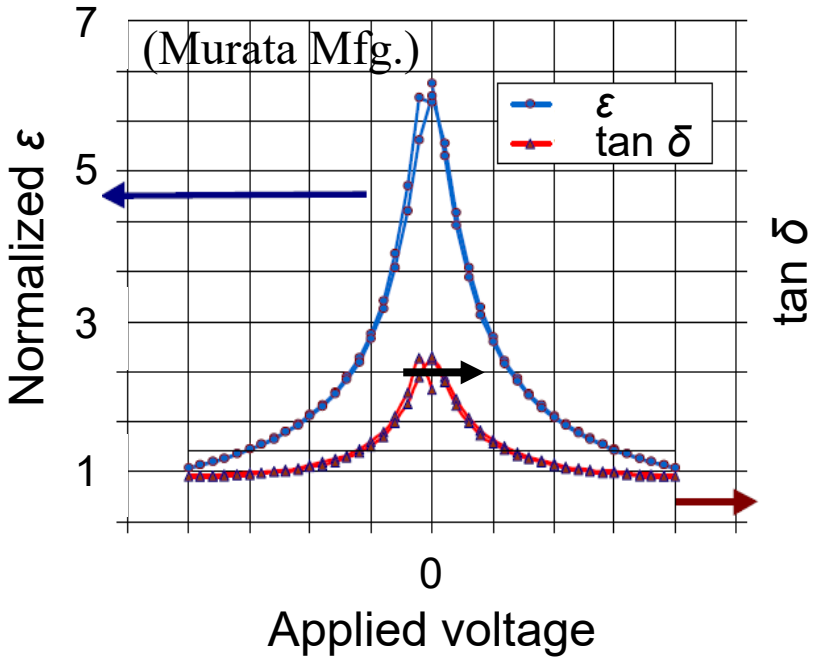

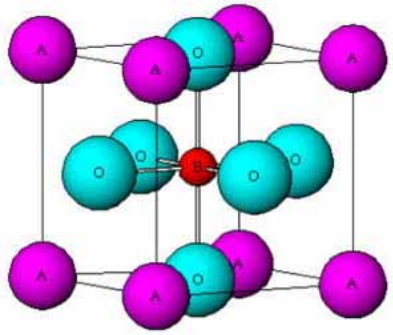

$(Ba_{1-x}Sr_x)TiO_3$

BST is deposited at 600ºC or higher.

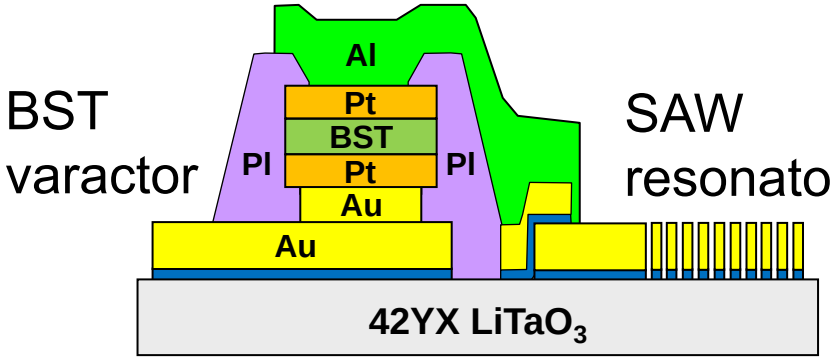

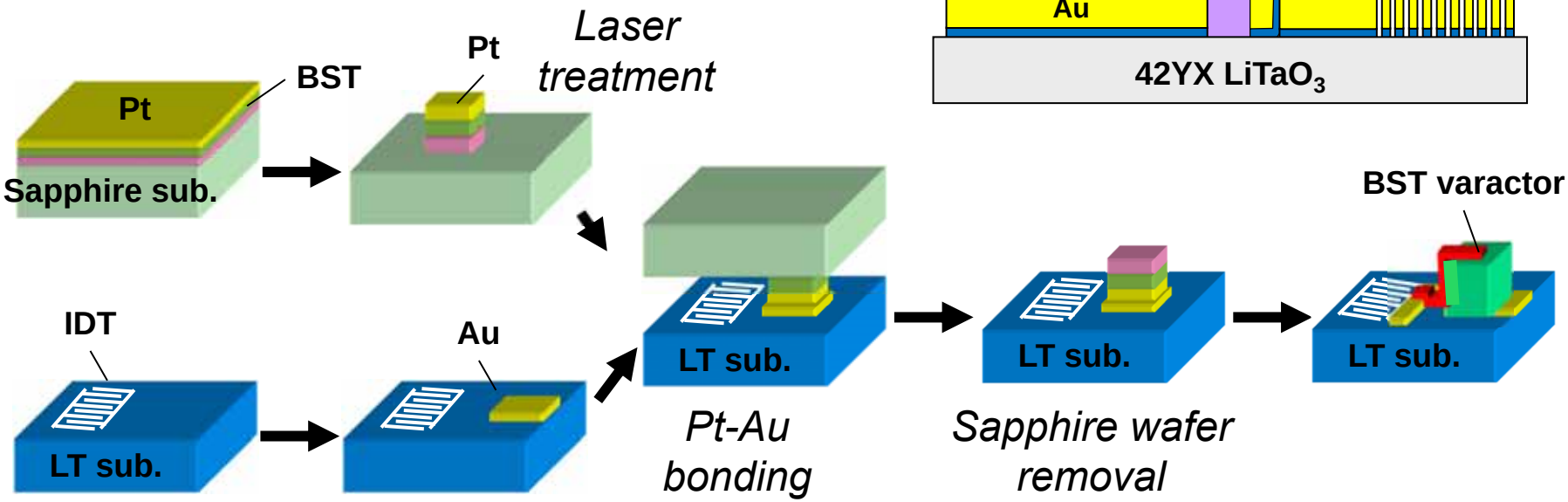

Transferred BST on LT SAW Wafer

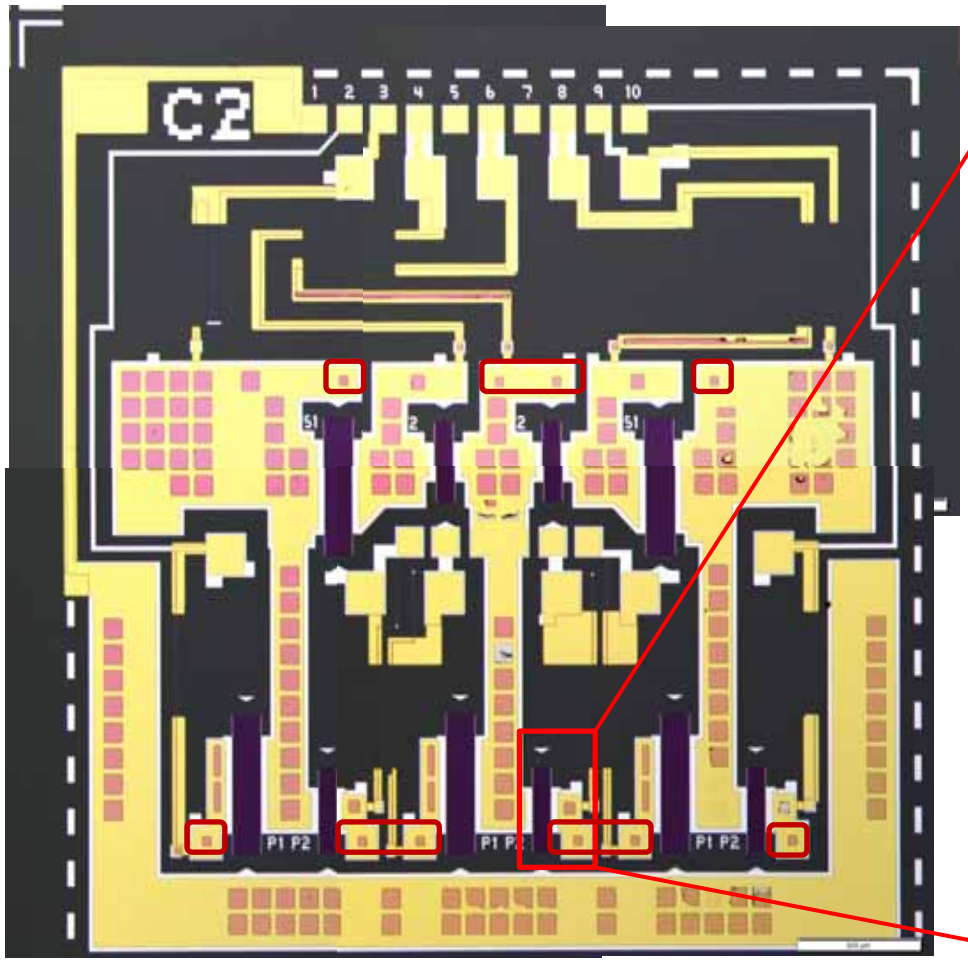

4 mm ✕ 4 mm

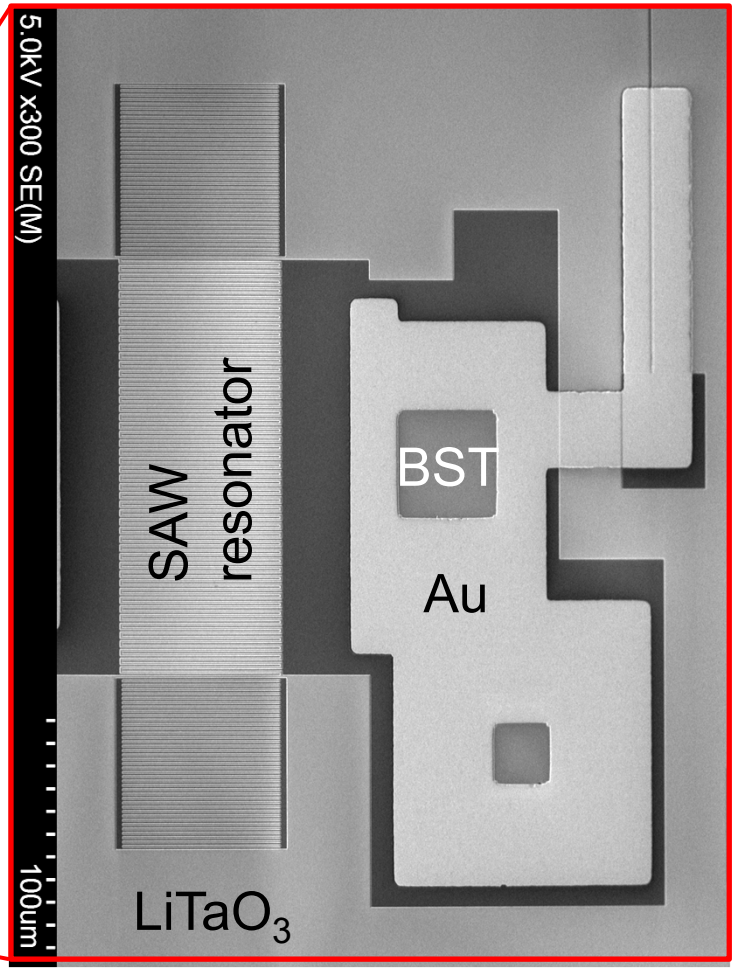

Bandpass Characteristic of Tunable SAW Filter

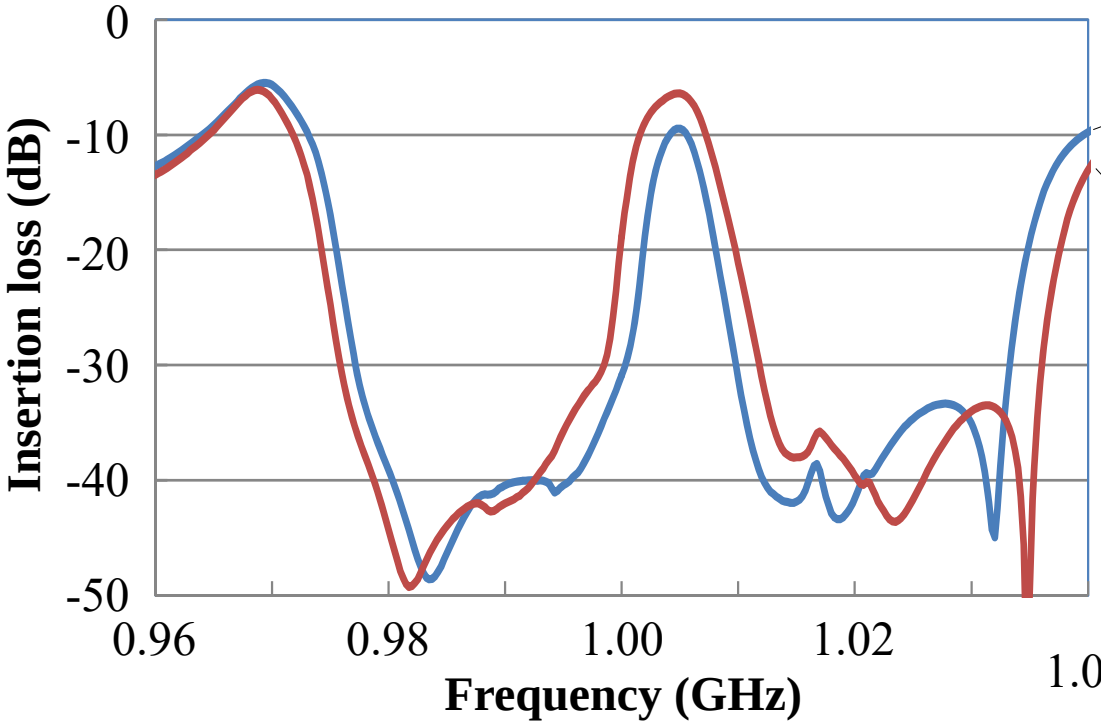

H. Hirano *et al.*, IEEE IUS 2014

C_{S1}, C_{P1}: 0 V, C_{S2}, C_{P2}: 7 V

C_{S1}, C_{P1}: 7 V, C_{S2}, C_{P2}: 0 V

← Measured bandpass characteristic

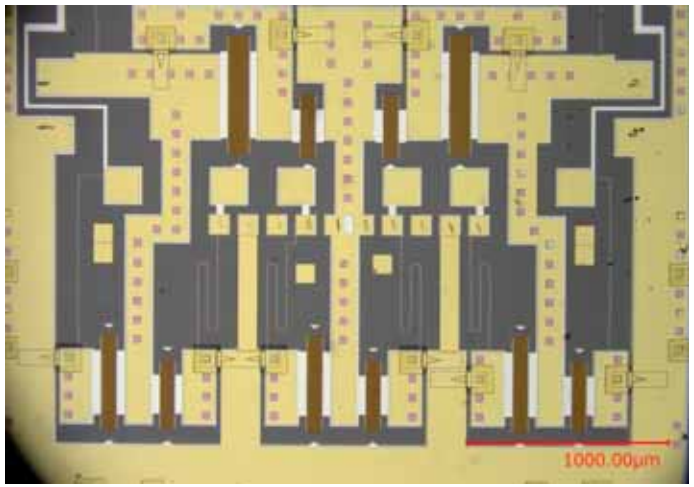

Designed bandpass characteristic ↓

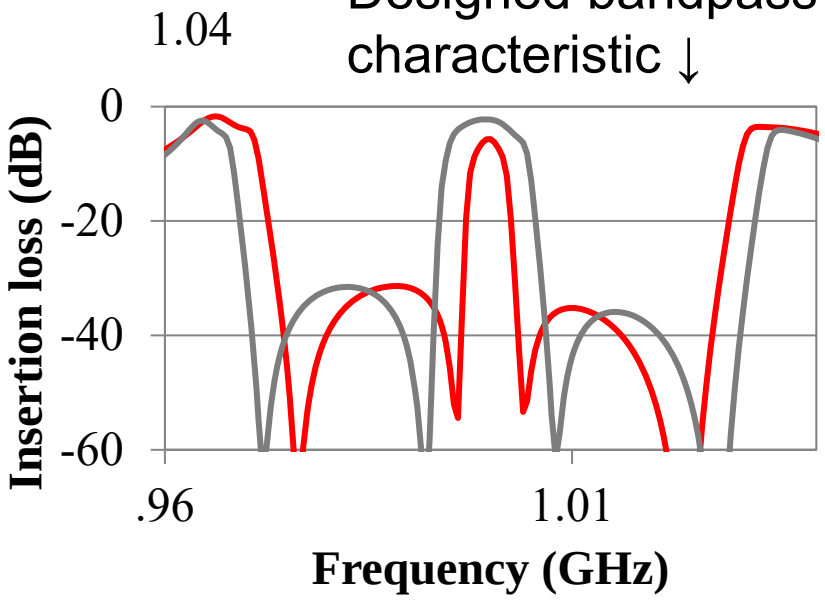

Demonstration Using Tunable SAW Filter

Connected using TV band

Cognitive wireless system
(Base station)

Tablet PC for interface connected to
the terminal cognitive wireless system

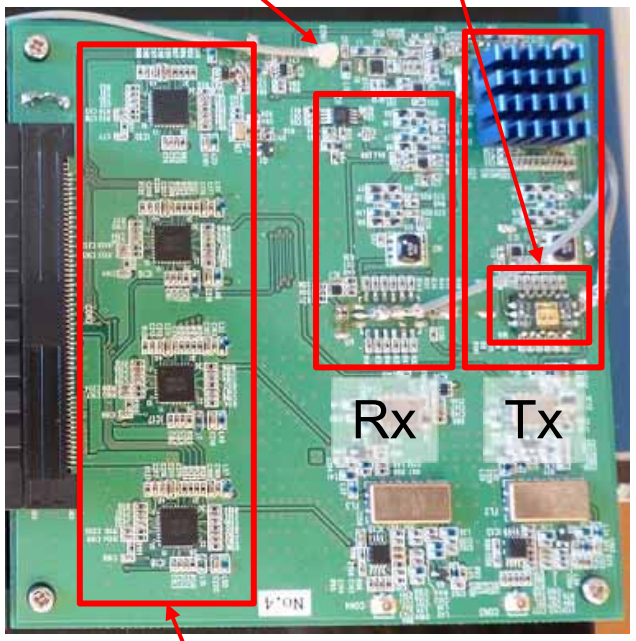

The cognitive wireless system was developed by NICT.

Requirements for BAW/SAW Filters

- Lager power handling ← LTE (Overlap of subcarrier)
- Smaller nonlinearity (Inter Modulation Distortion) ← Carrier aggregation
- Improvement of basic performance (IL, cut-off characteristic and TCF)
  ← Difficult-to-deal bands (e.g. LTE Band 25 and Band 11+21)
- Higher frequency for 5G (3.5~5 GHz)

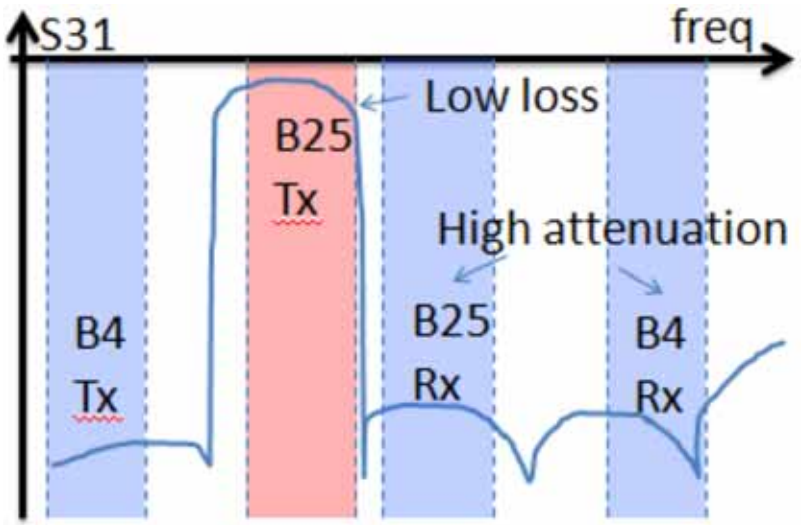

Band 25 Tx filter

T. Takai *et al.* (Murata Mfg.), IEEE IMS 2016

Up link: 1850〜1915 MHz (BW 65 MHz)
Down link: 1930〜1995 MHz (BW 65 MHz)
Guard band: 15 MHz → Extremely narrow

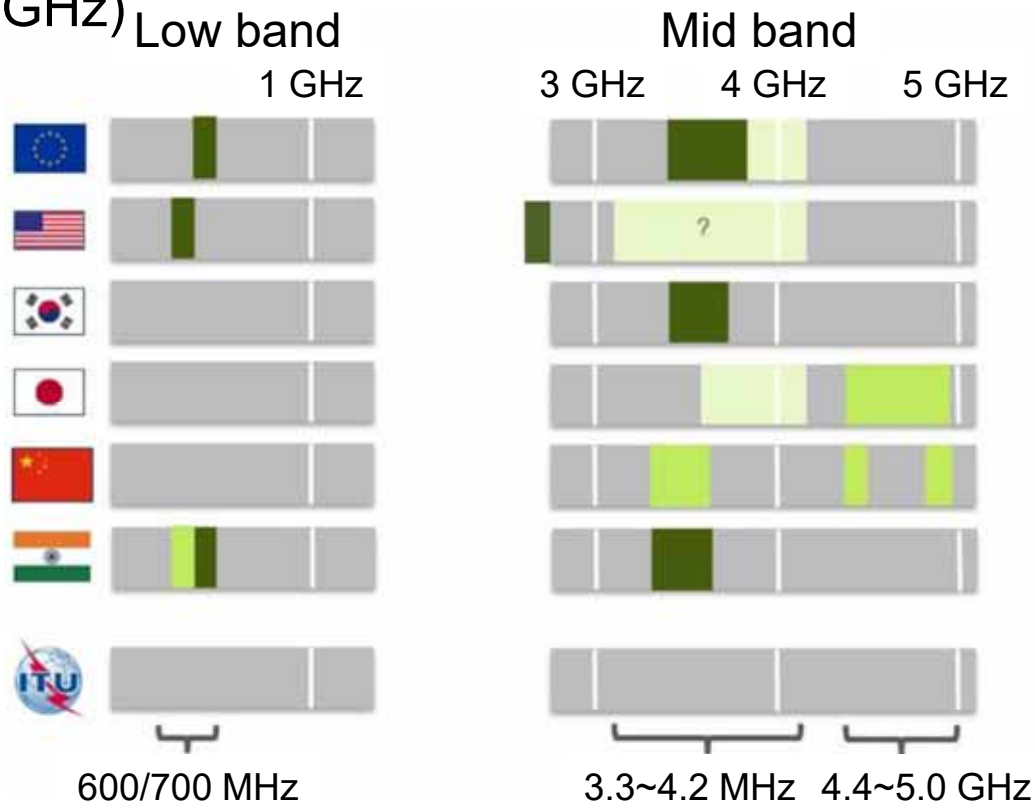

Balazs Bertenyi (Nokia),
Chairman of 3GPP RAN

Band n77 3.3~4.2 GHz
Band n78 3.3~3.8 GHz
Band n79 4.4~5.0 GHz

Acoustic Wave Devices Using Thin LT or LN

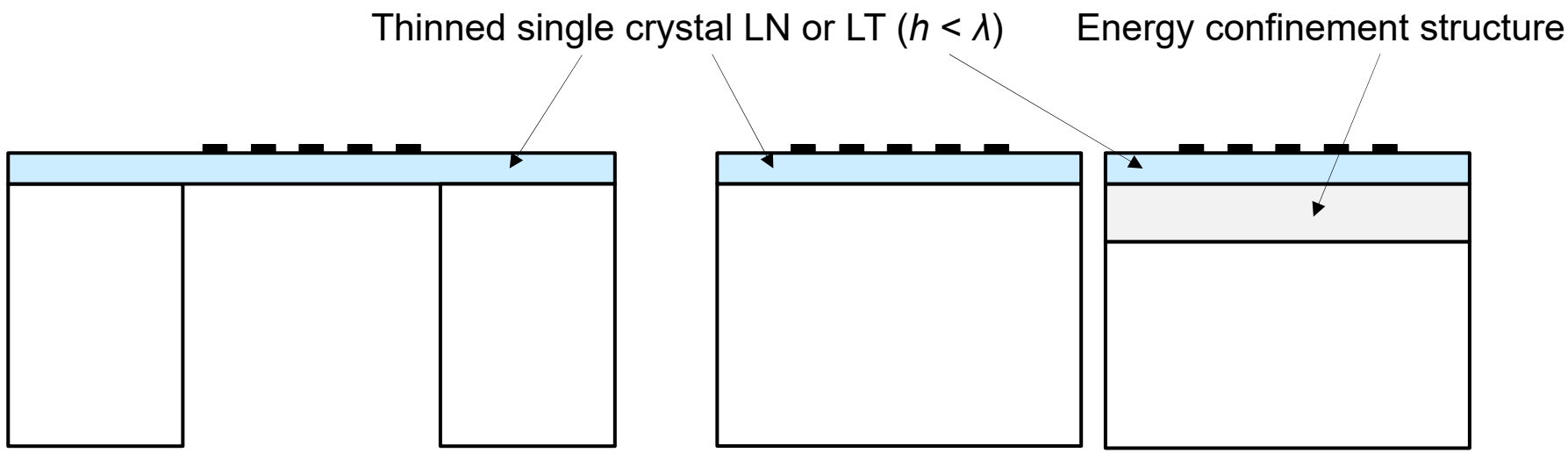

[1] M. Kadota *et al.*, IEEE Trans. UFFC, 57, 11 (2010)
[2] S. Gong, G. Piazza, IEEE Trans. MTT, 61, 1 (2013)
[3] R. Wang *et al.*, IEEE IFCS 2014
[4] M. Kadota, S. Tanaka, IEEE Trans. UFFC, 62 (2015) (SH mode)
[5] M. Kadota, S. Tanaka, Jpn. J. Appl. Phys., 55 (2016) (SH mode)
[6] N. Assila, M. Kadota, S. Tanaka, IEEE IFCS 2016 (A_1 mode)
[7] Y. H. Song, S. Gong, IEEE MEMS 2016

[1] T. Kimura, … M. Kadota, Jpn. J. Appl. Phys., 52 (2013) (S_0 mode)
[2] M. Kadota, S. Tanaka, Jpn. J. Appl. Phys., 54 (2015) (SH mode)
[3] M. Kadota, S. Tanaka, IEEE IFCS 2016 (SH mode)
[4] M. Kadota, S. Tanaka, IEEE IUS 2016 (SH mode)
[5] T. Takai *et al.*, IEEE IUS 2016 (SH mode)
[6] M. Gomi, … S. Kakio, USE 2016
[7] M. Kadota, S. Tanaka, IEEE IFCS 2017 (SH mode)

Plate Waves

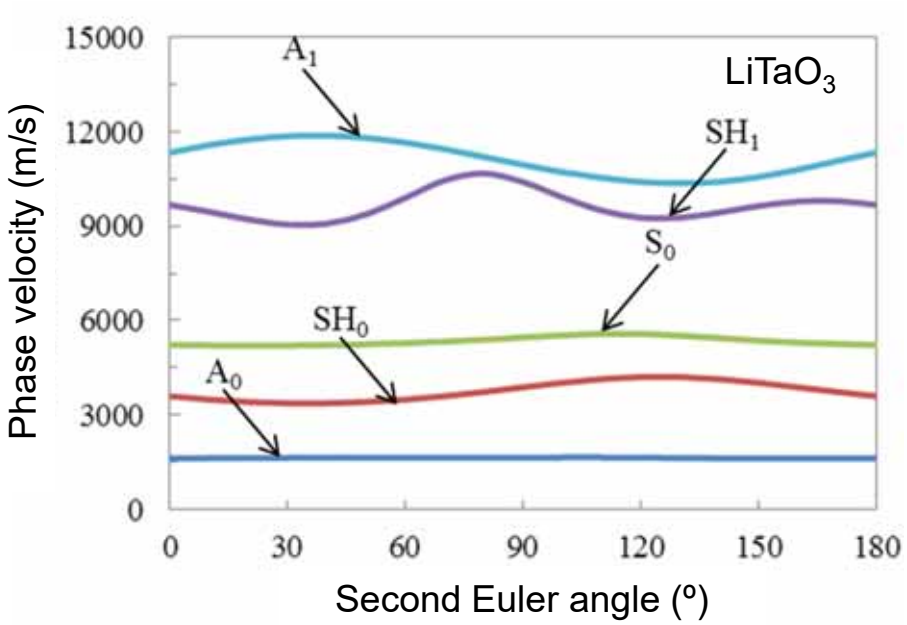

N. Assila, M. Kadota, S. Tanaka, IEEE IFCS 2016, pp. 365-368, Trans. UFFC, 66, 9 (2019) pp. 1529-1535

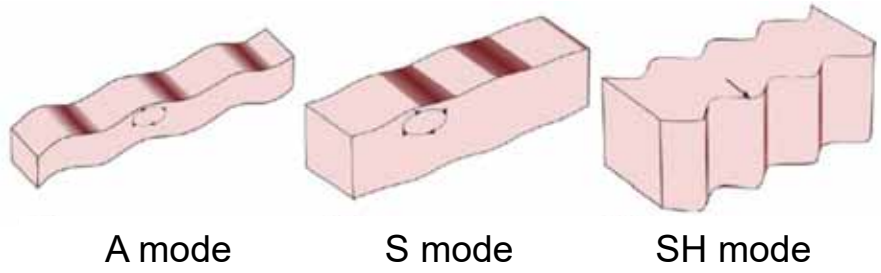

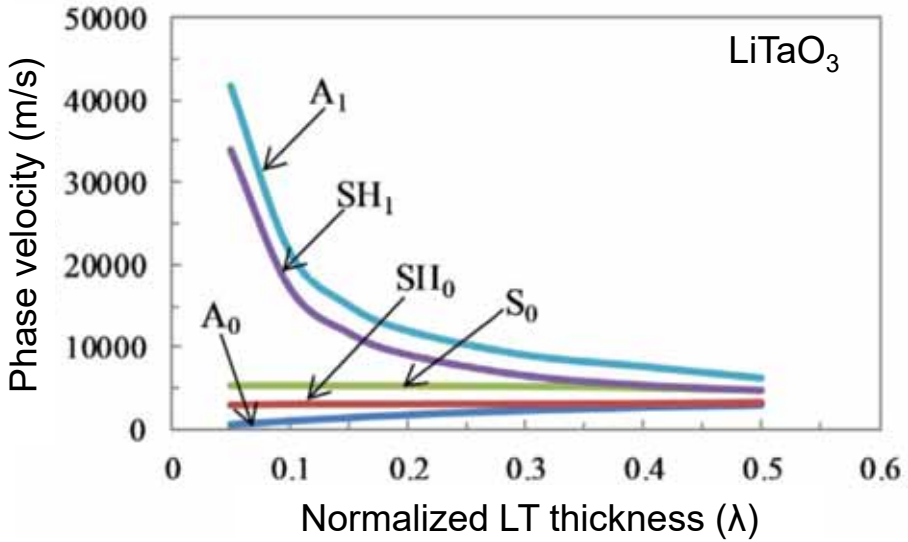

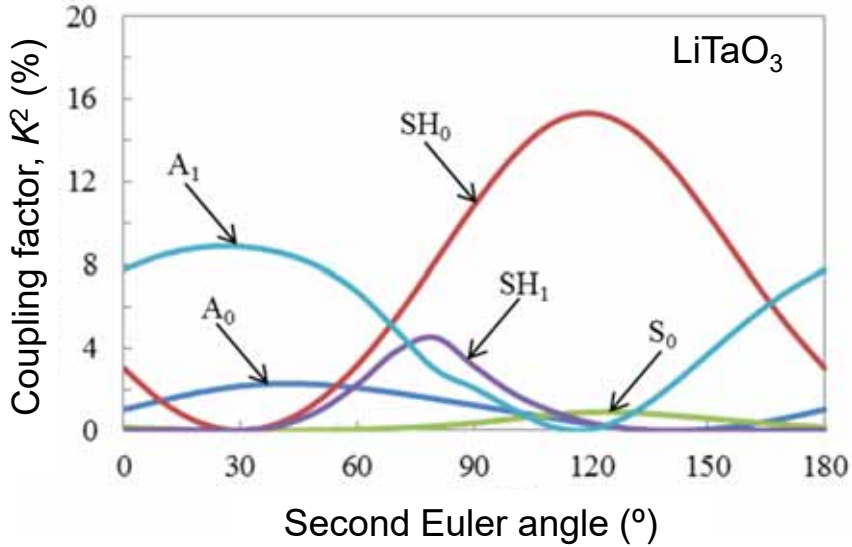

SH_0 Mode Ultrawideband Plate Wave Resonator

M. Kadota, S. Tanaka, IEEE Trans. UFFC, 62, 5 (2015) pp. 939-946
M. Kadota, S. Tanaka, Jpn. J. Appl. Phys., 55 (2016) 07KD04

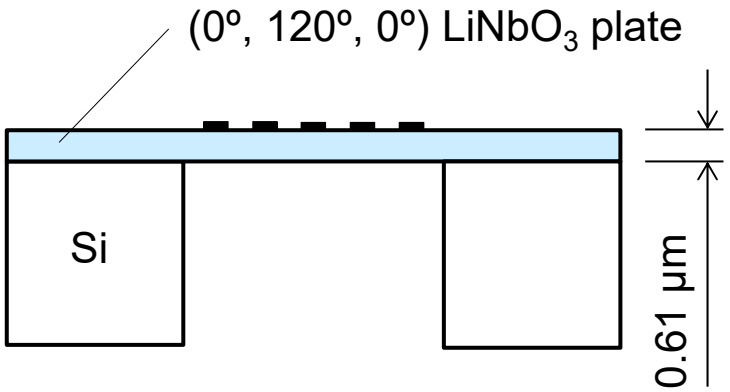

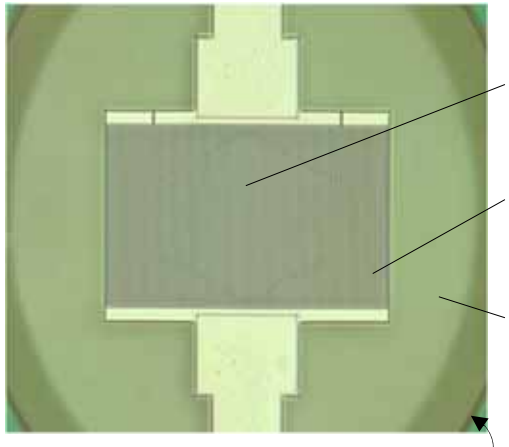

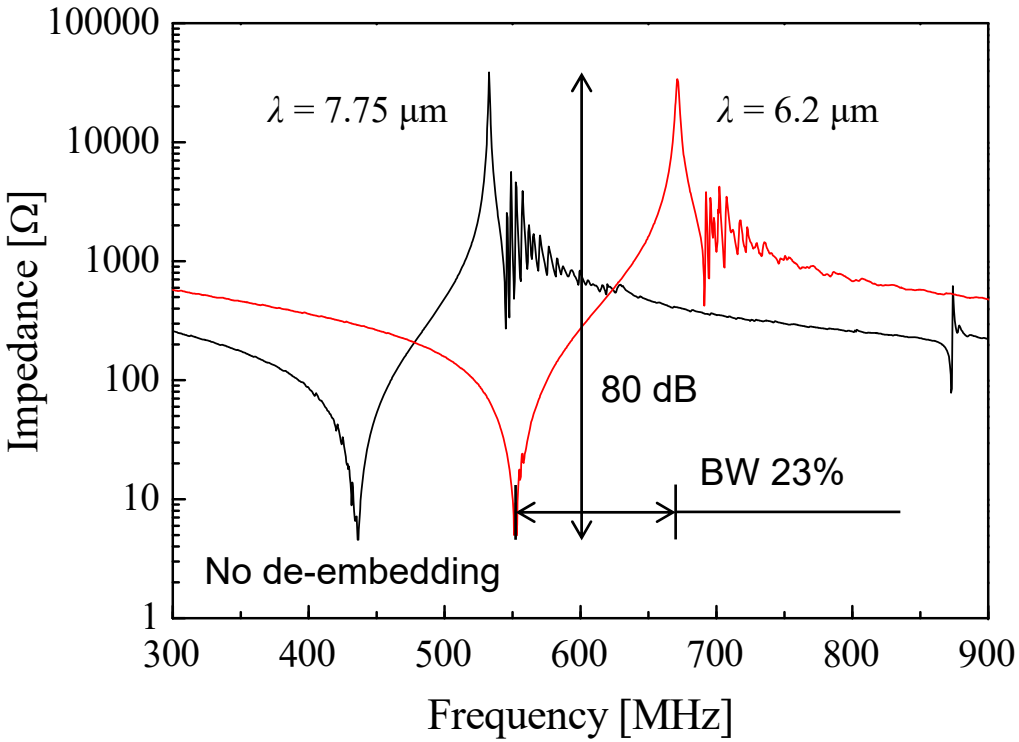

Coupling factor > 50%
Impedance ratio = 80 dB

A_1 Mode 5 GHz Plate Wave Resonator

N. Assila, M. Kadota, S. Tanaka, IEEE IFCS 2016, pp. 365-368
N. Assila, M. Kadota, S. Tanaka, Trans. UFFC, 66, 9 (2019) pp. 1529-1535

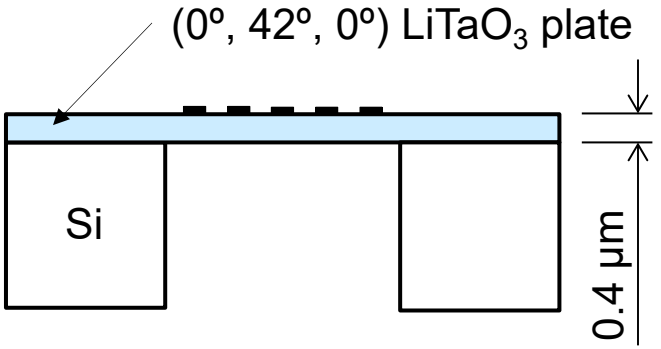

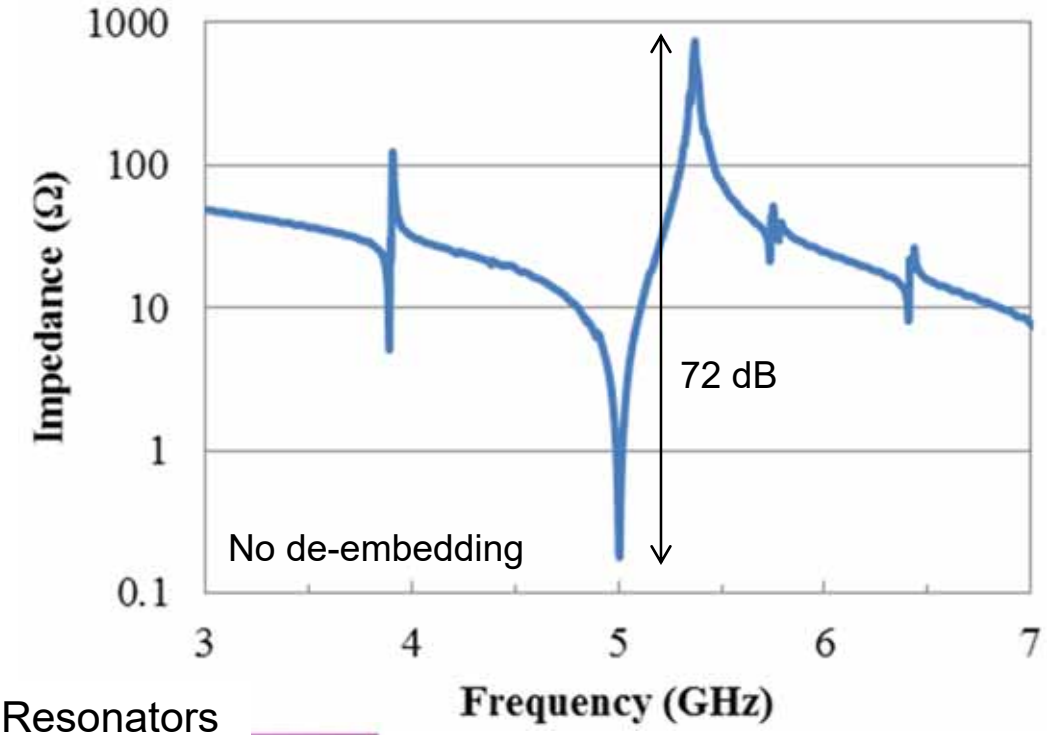

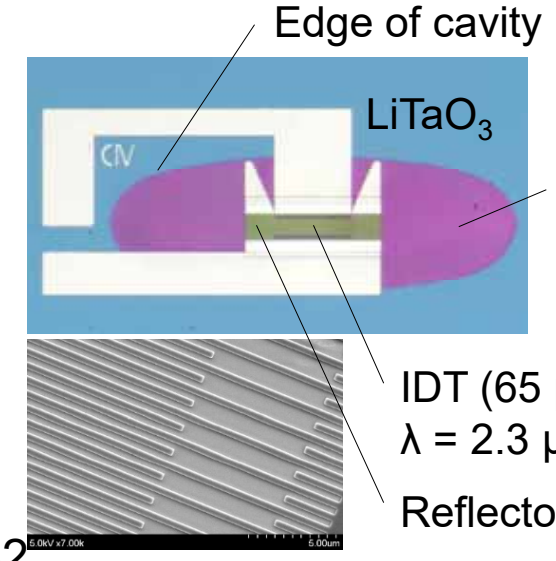

Resonators

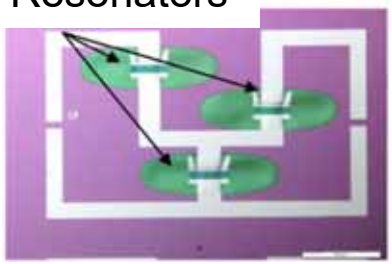

Coupling factor = 7.3%
Impedance ration = 72 dB
TCF = −43 ppm/K

Ultrawideband HAL SAW Resonator

M. Kadota, S. Tanaka, Jpn. J. Appl. Phys., 54 (2015) 07HD09
M. Kadota, S. Tanaka, Trans. UFFC, 62 (2015) M. Kadota, S. Tanaka, IEEE IUS 2016

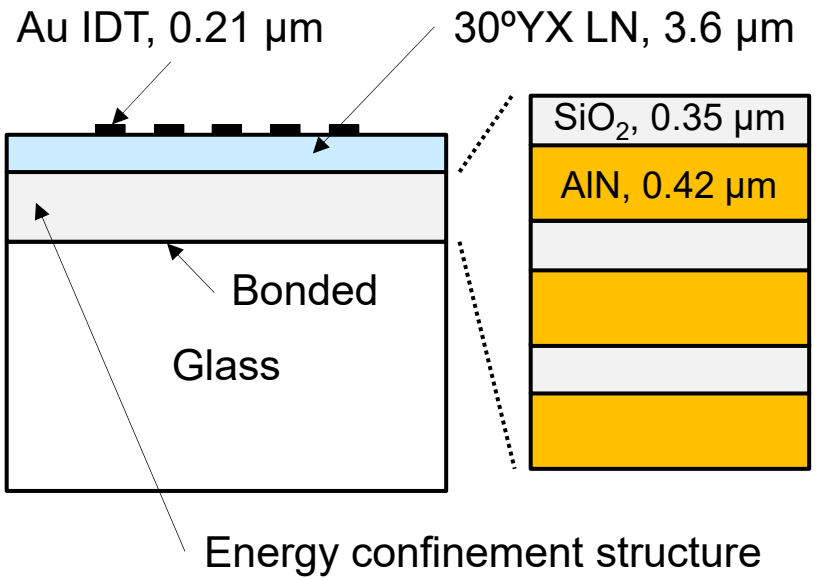

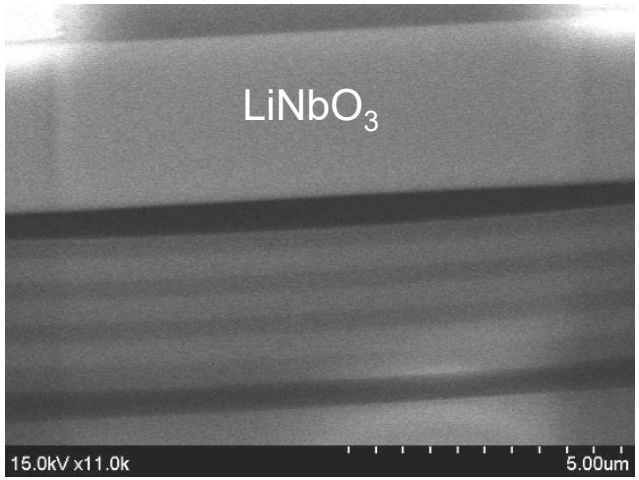

Energy confinement structure

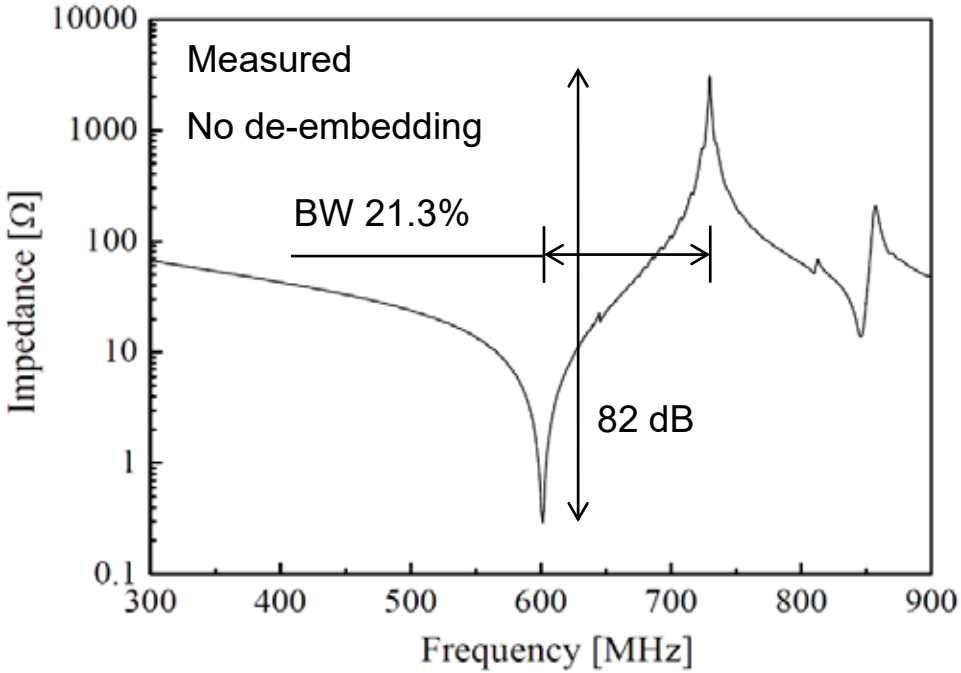

Impedance ratio = 82 dB
Bandwidth = 21.3%

Thin LT/Quartz HAL SAW Resonator

M. Kadota, S. Tanaka, IEEE International Ultrasonics Symposium 2017
M. Kadota, Y. Ishii, S. Tanaka, IEEE Trans. Ultrason. Ferroelectr. Freq. Contr., 68, 5 (2021) pp. 1955-1964

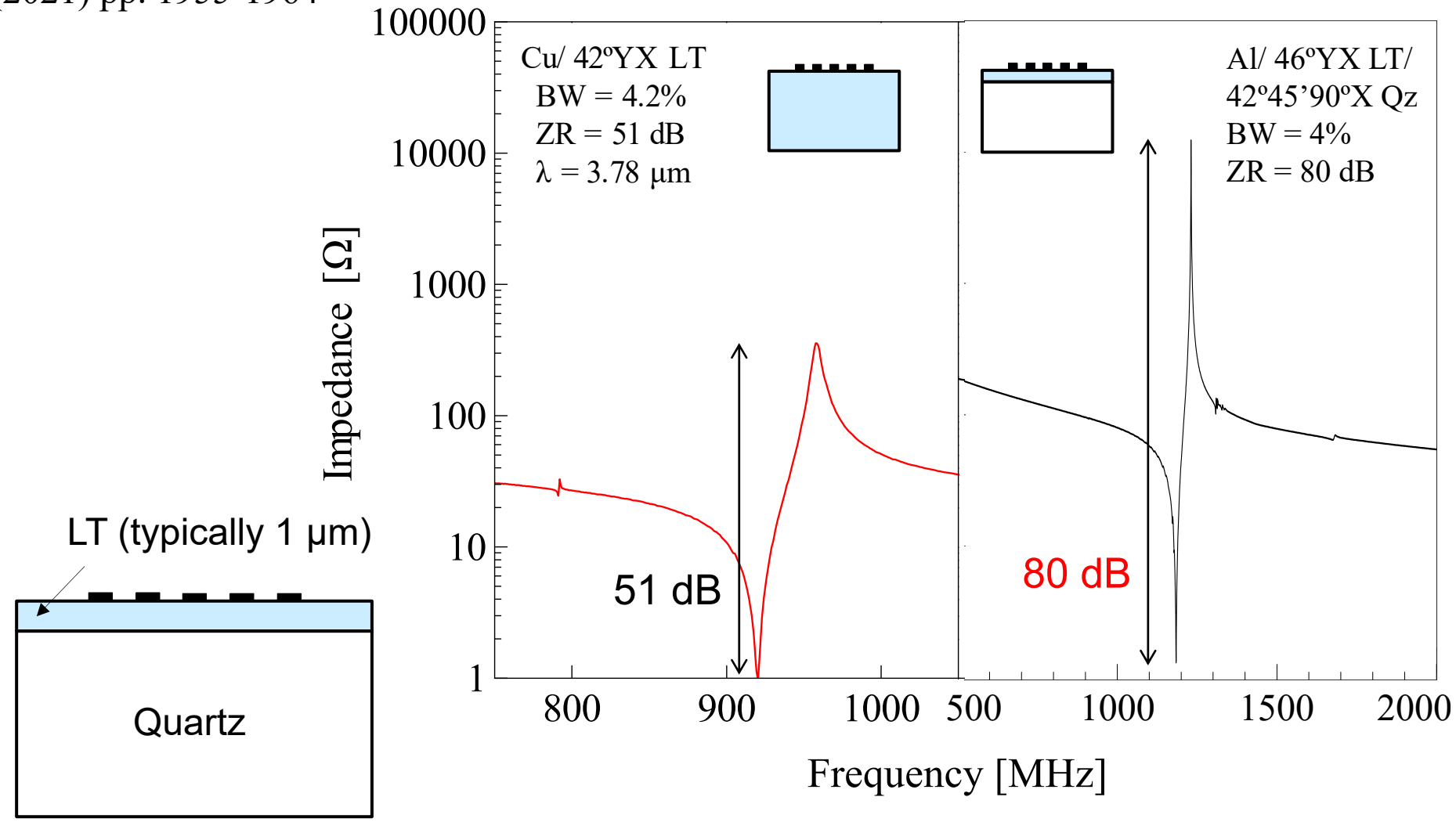

Near Zero TCF HAL SAW Resonator

M. Kadota … S. Tanaka, IEEE IFCS 2018
M. Kadota, Y. Ishii, S. Tanaka, IEEE Trans. Ultrason. Ferroelectr. Freq. Contr., 68, 5 (2021) pp. 1955-1964

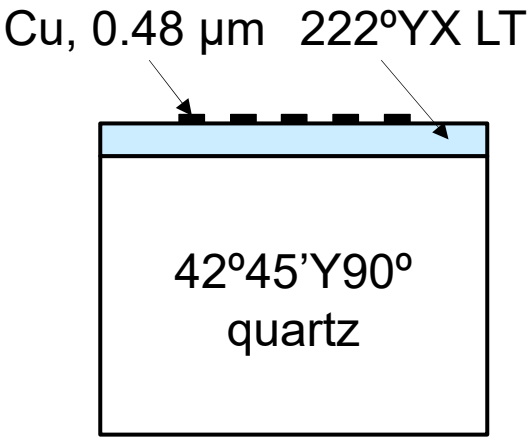

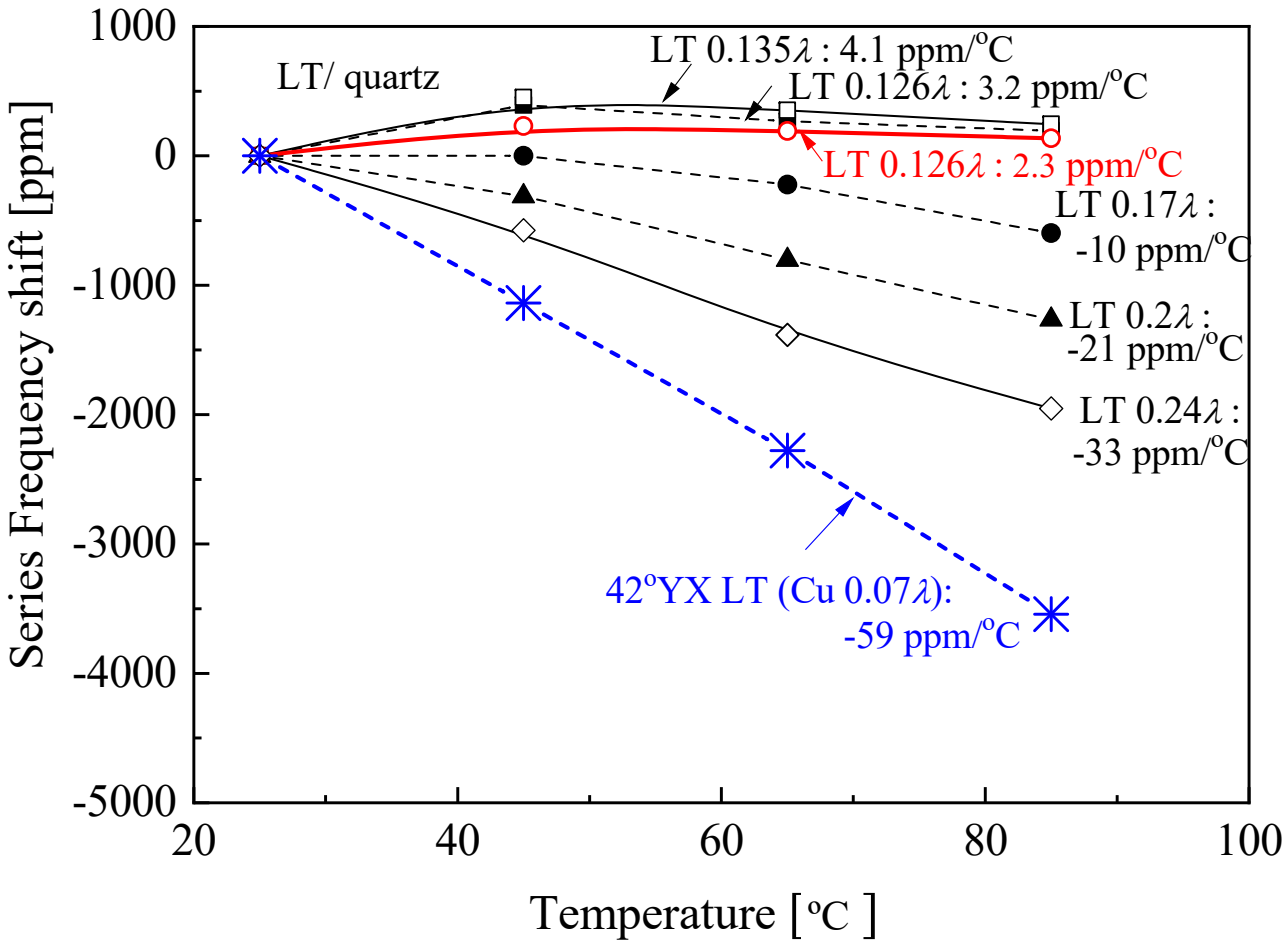

Measure temperature coefficient of series frequency of HAL SAW resonator with Cu IDT/ 222°YX LT/ 42°45'Y90°X structure

Integrated Tactile Sensor

mems tohoku

検索

Sensors Connected to Bus via Platform LSI

Conventional method

- ✓ Low density
- ✓ Busy wires
- ✓ Inconsistent interface
- ✓ Low performance especially for analog sensors

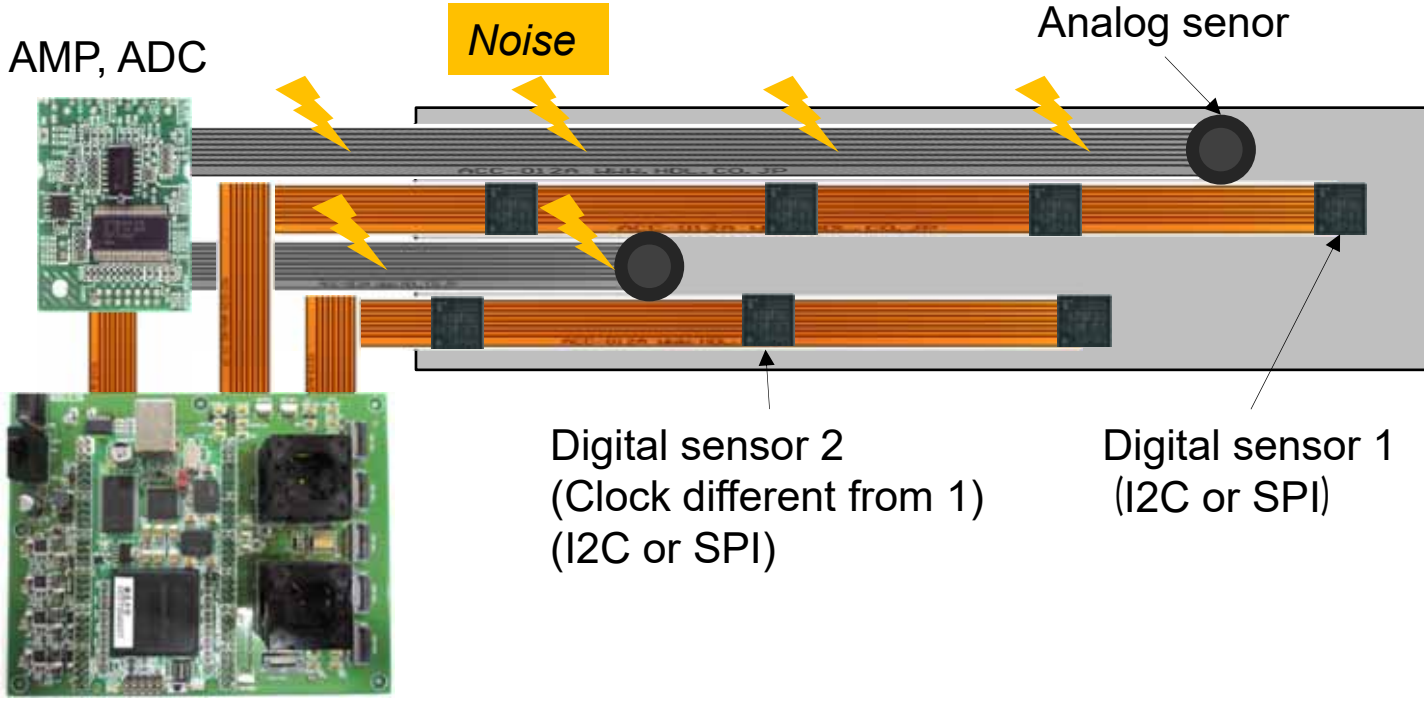

Platform LSI

- ✓ High density
- ✓ Minimum wires
- ✓ Consistent interface
- ✓ High performance
- ✓ Event driven

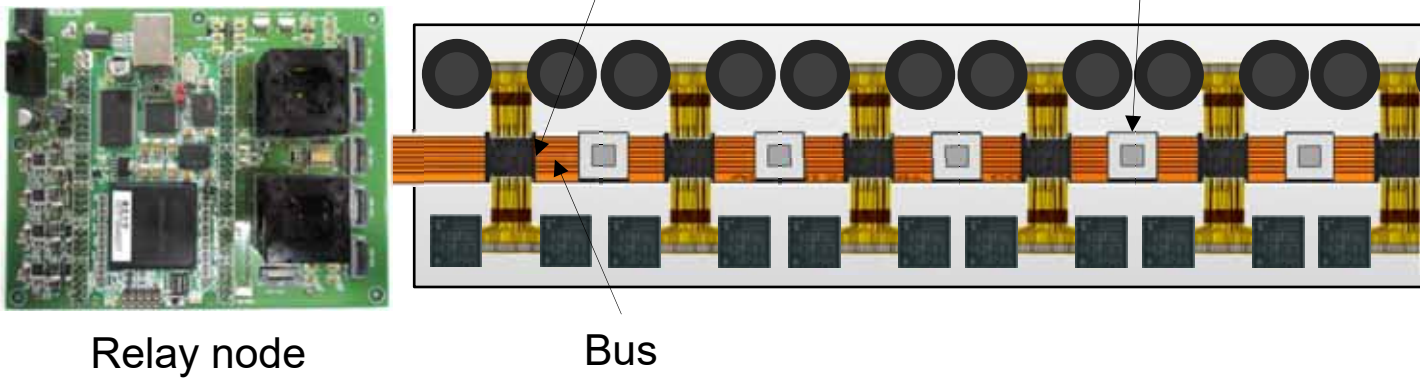

Demonstration of Event-Driven Operation

Please watch the student's finger(s) and the oscilloscope.
Only when the sensor is pushed, a packet appears on the oscilloscope.

Tactile Sensor Network Covers Robot Surface

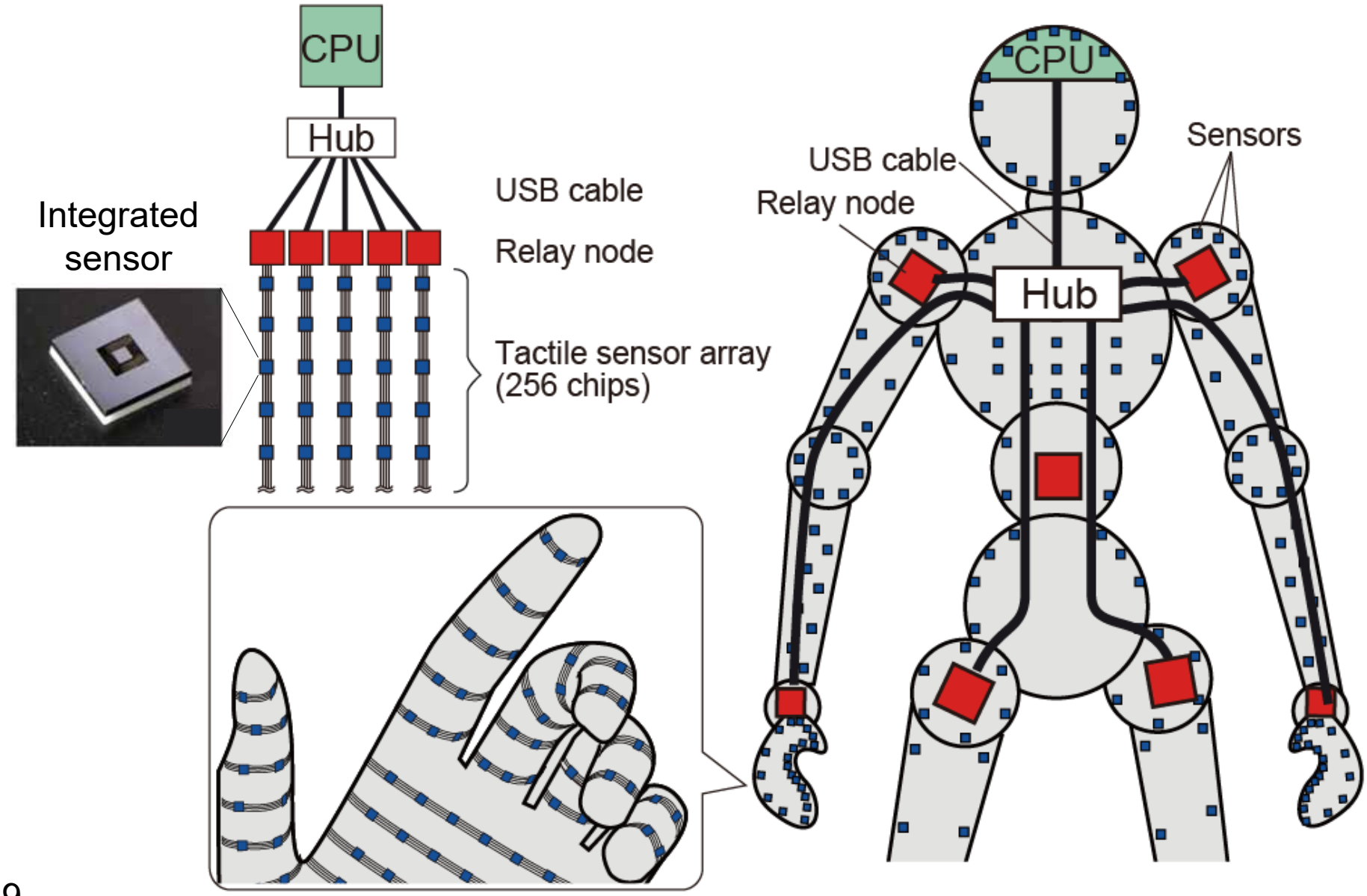

Integrated Finger Sensor (3 Axis Force + Temp)

Sho Asano *et al.*, IEEE MEMS 2016, pp. 850-853, Sensor Symposium 2016

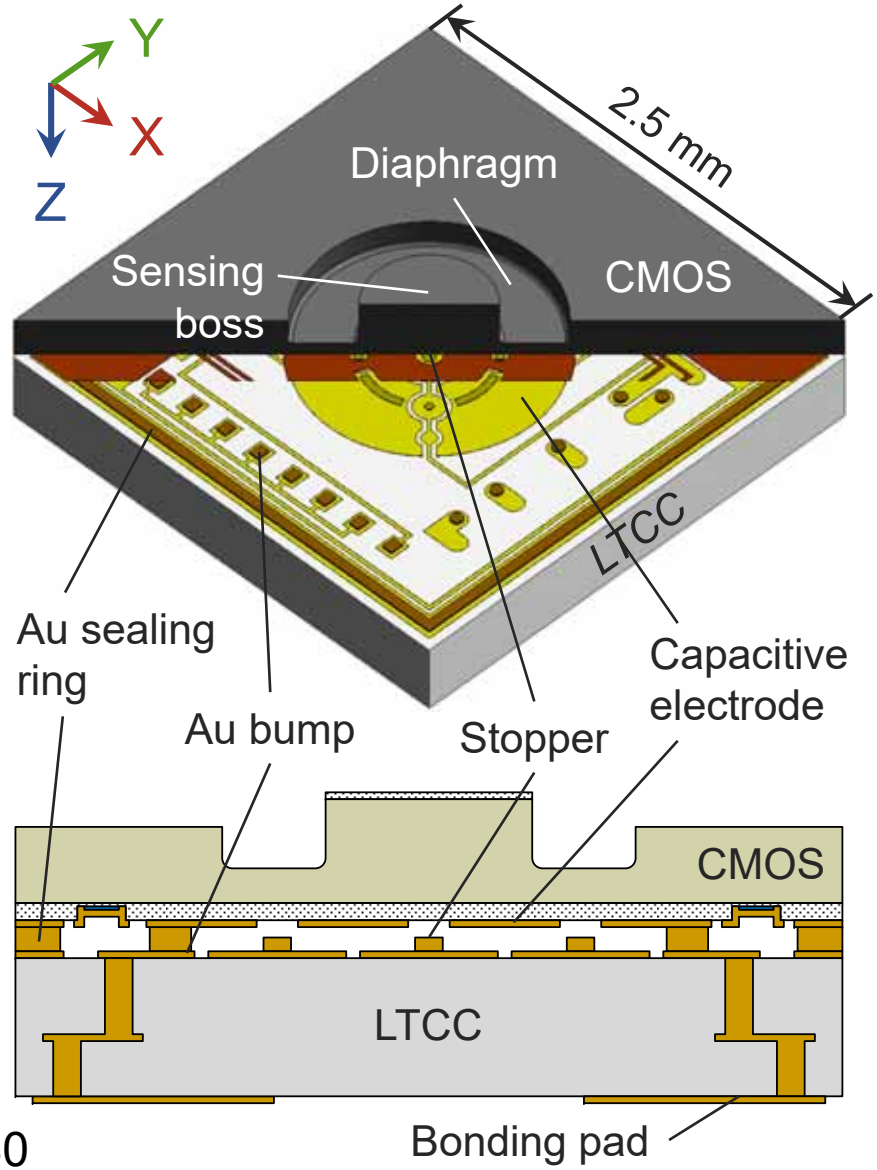

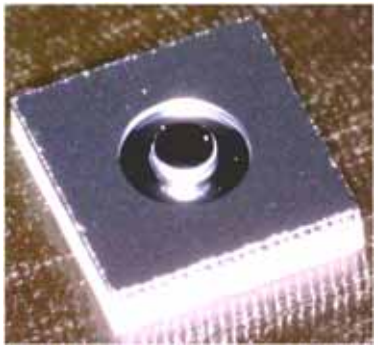

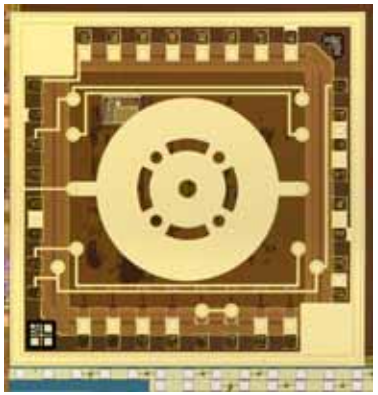

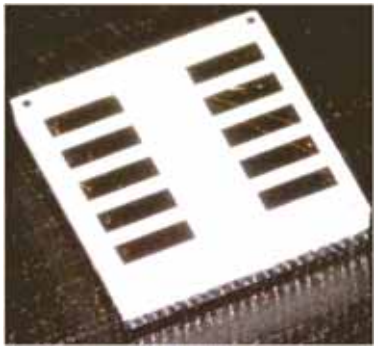

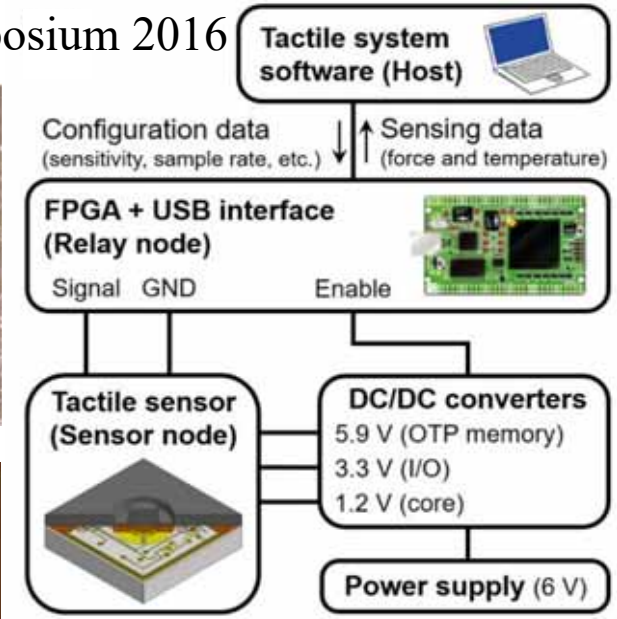

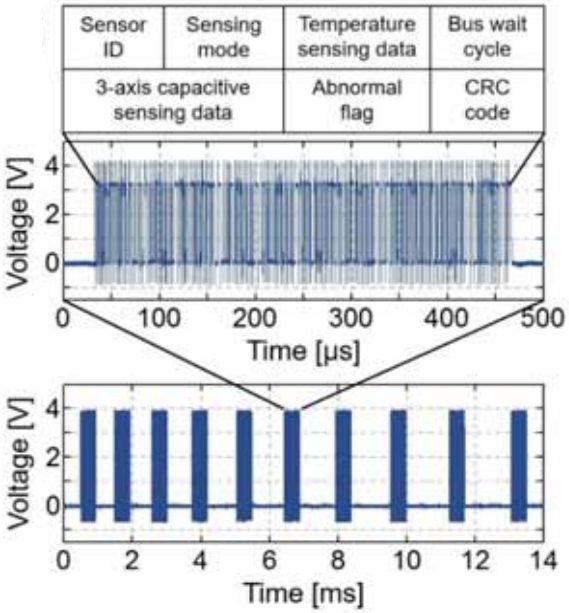

Integrated Tactile Sensor (Tohoku U + Toyota)

Yoshiyuki Hata *et al.* (Toyota CRL, Tohoku University, Toyota Motor), Transducers 2017, pp. 500-503

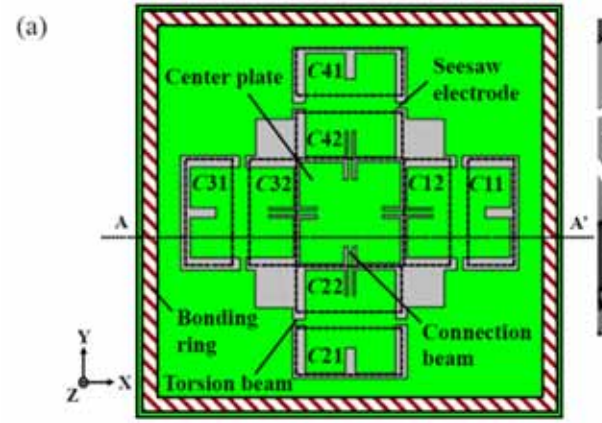

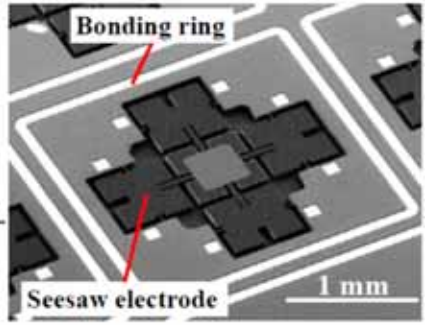

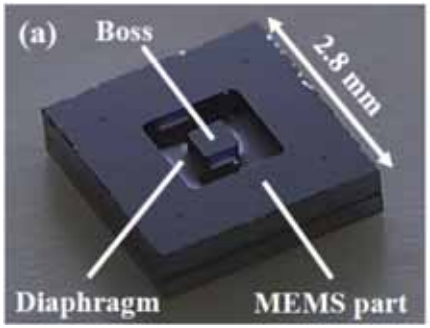

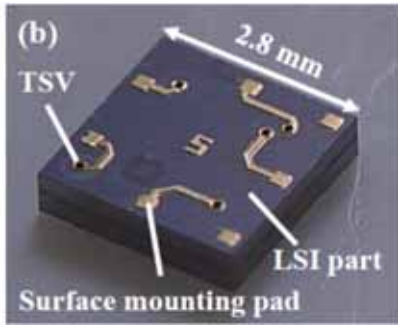

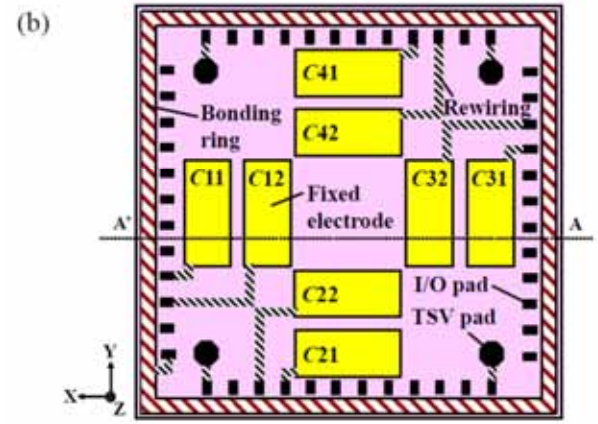

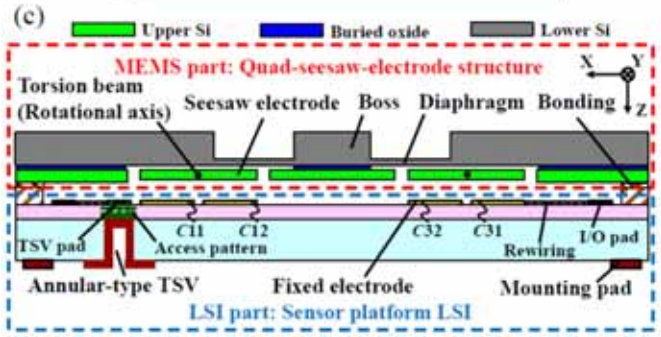

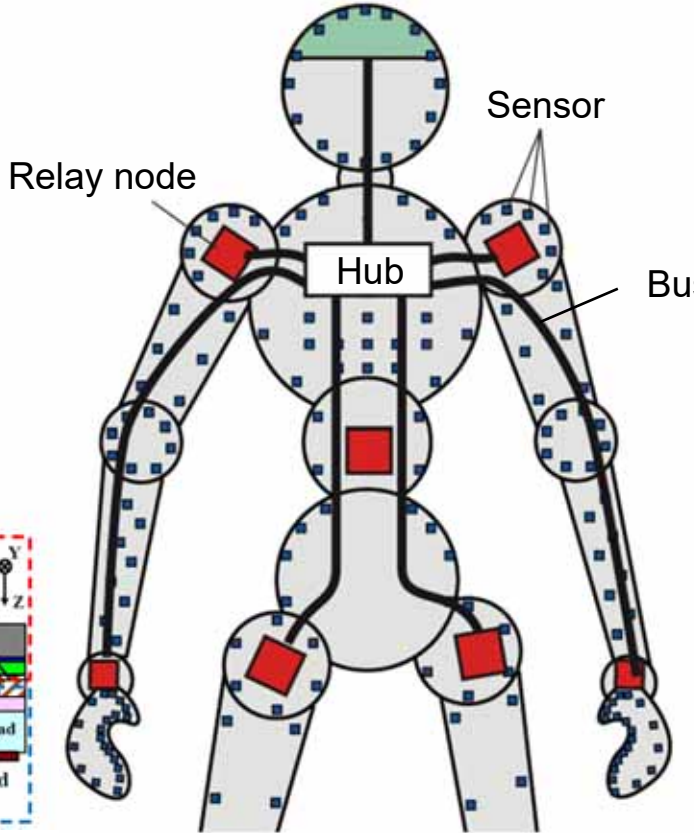

<u>Event driven operation</u>: Only the sensor which is stimulated sends a packet.

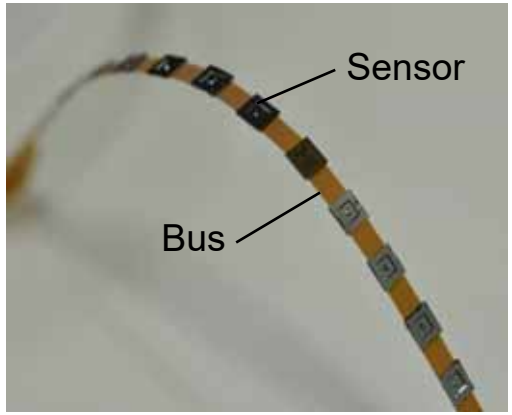

Our MEMS-LSI Integration Platform

Yukio Suzuki *et al.*, IEEE MEMS 2017, pp. 744-747
日経テクノロジーオンライン,「トヨタと東北大が新技術, ロボットセンサーとICを安

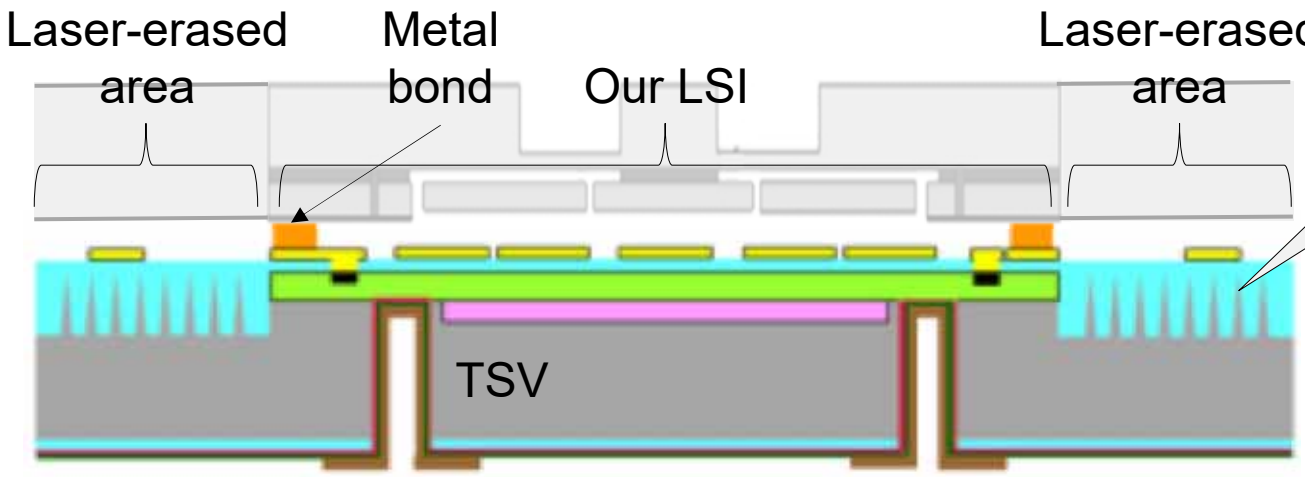

The LSI is produced on a shuttle wafer, and other customers' LSIs are erased by laser ablation.

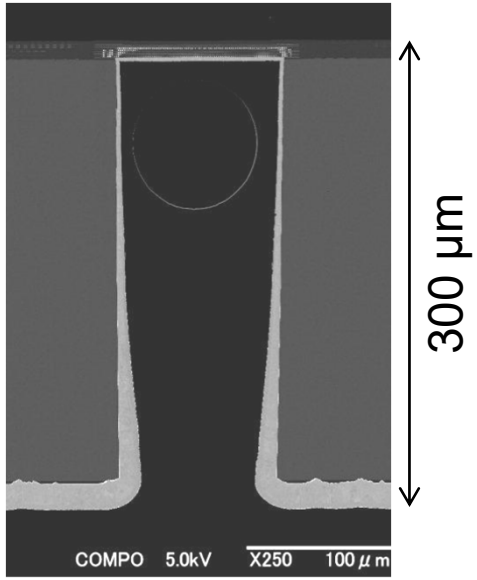

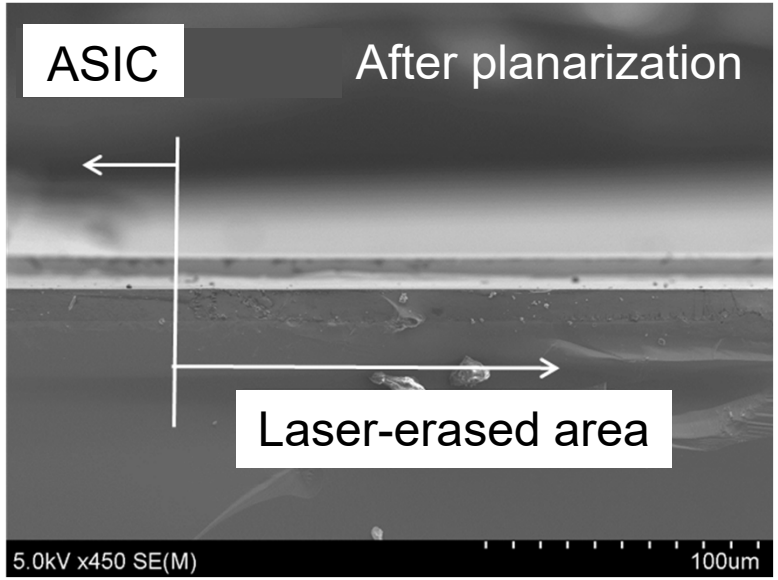

100 Integrated Sensors on Same Bus

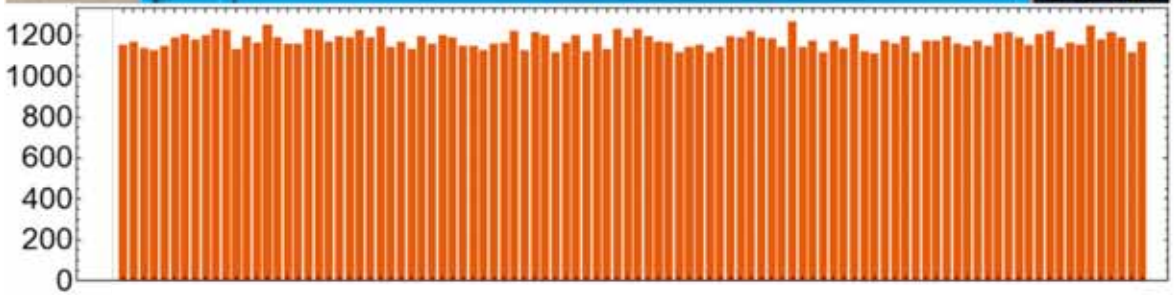

Number of packets received by each sensor in 30 s

Each PCB has 20 integrated tactile sensors on a bus.
5 PCBs are connected via the bus.

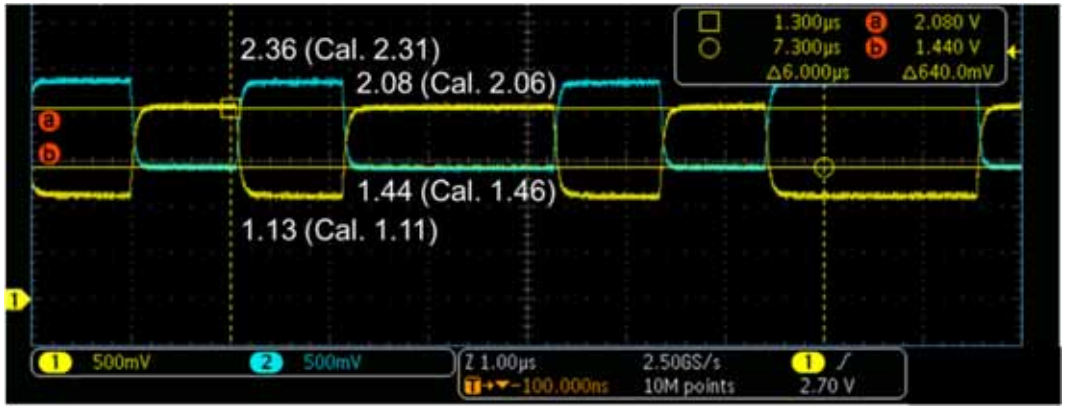

Signal on the bus

Summary Video

Example of Sensor Installation

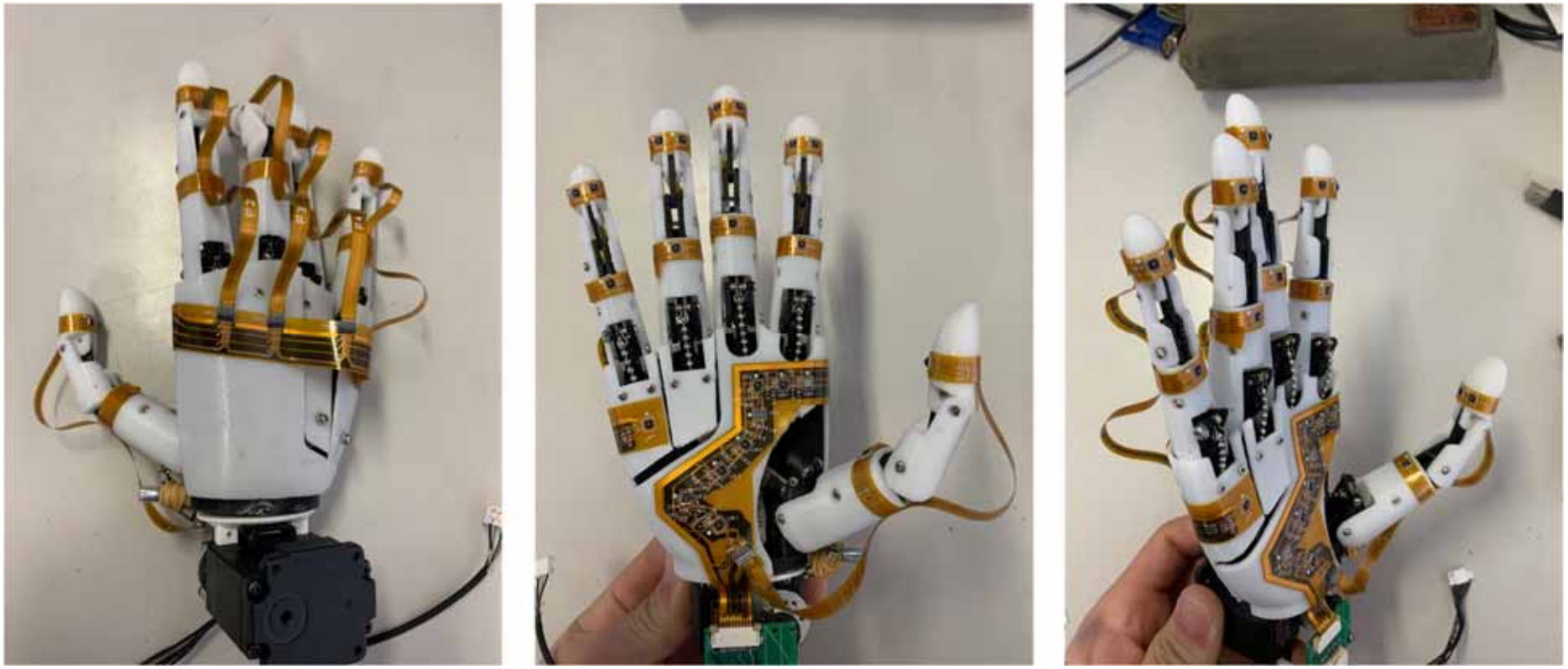

20 sensors on mechanical hand

S. Tanaka Laboratory

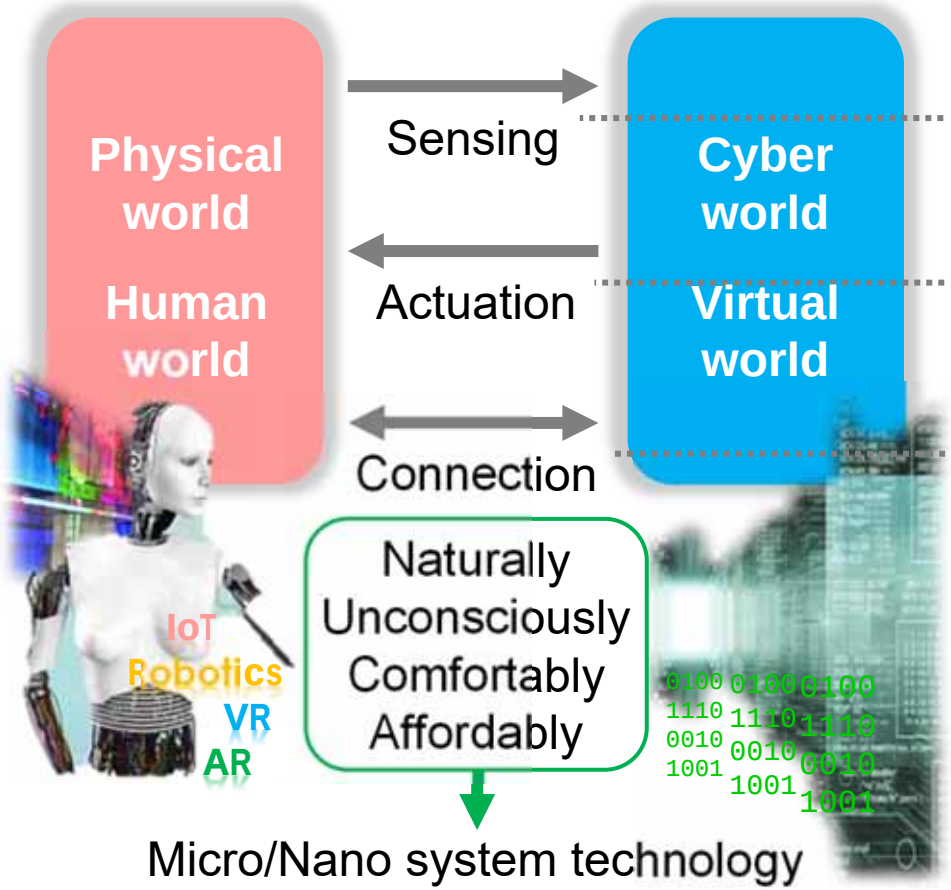

Research topics in 2018-2019

e.g. Tactile sensor, Gyroscope, Ultrasonic sensor, Microphone

e.g. Micromirror, Optical stage, RF MEMS switch

e.g. SAW and BAW filter

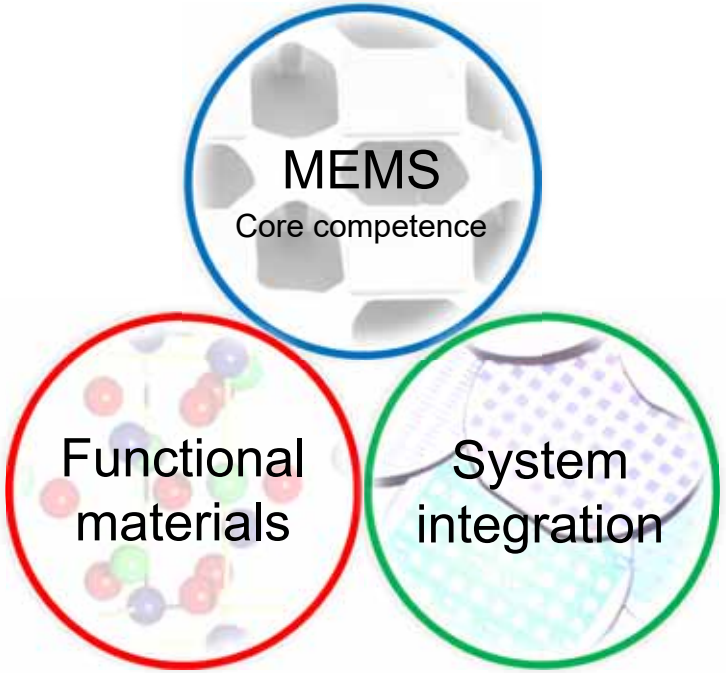

Recent research topics

Gyroscope, Ultrasonic transducer, Tactile sensor, Haptic device, MEMS speaker, Micromirror device, MEMS actuator stage, Acoustic wave device, Piezoelectric thin film, Packaging, ALD etc.

IMAC-G Program for International Students

http://www.imac.mech.tohoku.ac.jp/

If you are interested, please contact me earlier, one year before the entrance.
It is the timing to consider the entrance in October 2022.

THE 35TH IEEE INTERNATIONAL CONFERENCE ON MICRO ELECTRO MECHANICAL SYSTEMS

MEMS TOKYO 2022 JAPAN

9 - 13 JANUARY 2022

9-13 January 2022, Tokyo, Japan

We invite and welcome you to joins us for the 35th International Conference on Micro Electro Mechanical Systems (IEEE MEMS 2022) that will be held **in-person** in **Tokyo, Japan**, as well as **virtually** for **online participation**. With the evolving circumstances regarding the global pandemic, we are currently preparing a conference schedule that is dynamic and engaging no matter the participation level.

The MEMS Conference thrives on the rapid proliferation MEMS technology that largely stems from the commitment and success of the microsystems research community as well as a bustling industrial community. In recent years, the IEEE MEMS Conference has attracted more than 700 participants with 800+ abstract submissions and has created an effective forum to present over 200 select papers in podium and poster/oral sessions. For 2021, we will continue a combination of single and parallel sessions provides ample opportunity for interaction between attendees, presenters and exhibitors.

Conference Chairs

Zhihong Li
Peking University, CHINA

Shuji Tanaka
Tohoku University, JAPAN

MEMS
IEEE MEMS TECHNICAL COMMUNITY

IEEE